UNIVERSITY OF Nebraska Lincoln

THE UNIVERSITY OF IOWA

KU THE UNIVERSITY OF KANSAS

MISSOURI S&T

LINCOLN UNIVERSITY MISSOURI

NICC

UNIVERSITY OF Nebraska Omaha

University of Nebraska Medical Center

KU MEDICAL CENTER The University of Kansas

Development of New Design Guidelines for Protection against Erosion at Bridge Abutments - Phase V

George Constantinescu, PhD
Professor
Department of Civil and Environmental Engineering
The University of Iowa

Hao Wu
Graduate Research Assistant
Department of Civil and Environmental Engineering
The University of Iowa

THE UNIVERSITY OF IOWA

2023

MATC

Development of New Design Guidelines for Protection against Erosion at Bridge Abutments - Phase V

George Constantinescu, Ph.D., PI
Professor
Department of Civil and Environmental Engineering
The University of Iowa

Hao Wu
Graduate Research Assistant
Department of Civil and Environmental Engineering
The University of Iowa

Technical Report Documentation Page

1. Report No. 25-1121-0005-141-5	2. Government Accession No.	3. Recipient's Catalog No.	
4. Title and Subtitle Development of New Design Guidelines for Protection against Erosion at Bridge Abutments - Phase V		5. Report Date May 2023	
		6. Performing Organization Code	
7. Author(s) George Constantinescu, Ph.D., PI ORCID: https://orcid.org/0000-0001-7060-8378 Hao Wu		8. Performing Organization Report No. 25-1121-0005-141-5	
9. Performing Organization Name and Address Department of Civil and Environmental Engineering The University of Iowa Iowa City, IA 52242		10. Work Unit No.	
		11. Contract or Grant No. 69A3551747107	
12. Sponsoring Agency Name and Address Mid-America Transportation Center 2200 Vine St. PO Box 830851 Lincoln, NE 68583-0851		13. Type of Report and Period Covered Final Report Jan 2022 – May 2023	
		14. Sponsoring Agency Code MATC TRB RiP No. 91994-97	
15. Supplementary Notes Conducted in cooperation with the U.S. Department of Transportation, Federal Highway Administration.			
16. Abstract Maintaining road operations requires reliable and safe transportation infrastructure design, in particular for bridges that need to remain operational during floods and other extreme weather events. A numerically based investigation is carried out to determine the critical discharge and Froude number to avoid shear failure inside the riprap apron used to protect spill-through and wing-wall abutments against erosion. The focus is on cases when the flow regime is pressurized at the bridge site. The Year 5 Report discusses how the bed shear stress distributions induced over the riprap apron protecting wing-wall and spill-through abutments placed in a straight compound channel vary with increasing flow depth. The study considered cases where the flow at the bridge site is in the free-surface (FS) flow regime and in the pressurized flow (submerged orifice or overtopping) regime. This data is critical to propose corrections to existing design formulas for riprap size selection which were developed only for the free-surface flow regime such that estimates of the critical Froude number can be provided for cases when the bridge deck becomes submerged at high flow conditions.			
17. Key Words Bridges, Bridge scour, Bridge abutment, Local Scour, Rip-rap protection against scour		18. Distribution Statement No restrictions. This document is available through the National Technical Information Service, Springfield, VA 22161.	
19. Security Classif. (of this report) Unclassified	20. Security Classif. (of this page) Unclassified	21. No. of Pages 47	22. Price

Form DOT F 1700.7 (8-72)   Reproduction of completed page authorized

Table of Contents

List of Figures

List of Tables

Acknowledgments

Disclaimer

The contents of this report reflect the views of the authors, who are responsible for the facts and the accuracy of the information presented herein. This document is disseminated in the interest of information exchange. The report is funded, partially or entirely, by a grant from the U.S. Department of Transportation's University Transportation Centers Program. However, the U.S. Government assumes no liability for the contents or use thereof.

Abstract

Severe floods in the United States Midwest have caused major erosion at bridge abutments despite their protection design measures following existing guidelines (e.g., HEC 23, 2001 and following updates through 2009). As the discharge and stage increase due to high flow conditions in the river, the near-bed velocities increase in the contracted flow region where the bridge abutments are situated (Sturm and Janjua, 1994; Sumer and Fredsoe, 2002). Placing riprap stone around the base of each abutment is the most common way to protect abutments against erosion (e.g., see NCHRP Projects 24-18, 24-19, 24-20). Existing design formulas to calculate the minimum size of the riprap stone used for protection of wing-wall and spill-through abutments (Lagasse et al., 2001; Pagan-Ortiz, 1991) are based on an oversimplified approach and do not account for complexities associated with these structures being placed in natural streams where, for instance, bank curvature effects may be important. The coefficients in these formulas were determined based on a limited series of laboratory experiments conducted for a relatively narrow range of relevant geometrical and flow parameters that control the capacity of the flow to induce erosion at such bridge sites. Another important limitation of present design formulas is that they can be applied only for open channel flow (free surface, FS) regime at the bridge site. However, the most severe scour around the abutments occurs when the bridge deck becomes submerged and the flow regime becomes pressurized (e.g., submerge orifice, SO, regime or overtopping, OT regime).

The proposed approach to study flow around spill-though and wing-wall abutments protected by a riprap apron and to estimate the critical Froude number for riprap entrainment is based on a numerical approach. The mean flow fields and the bed shear stress distributions are obtained from fully three-dimensional, non-hydrostatic RANS simulations. These data are then

used to estimate the maximum bed shear stress over the riprap apron, the shear-failure entrainment threshold for the riprap stone and the other variables in the design formulas recommended in HEC 23. The approach was validated for the case of wing-wall abutments placed in a straight channel based on data from laboratory experiments.

The main goal of the project is to improve the performance and range of applicability of riprap design formulas used for erosion protection at wing-wall and spill-through abutments by extending the range of applicability of existing design formulas for cases when the channel curvature at the bridge site is sufficiently high to affect the critical Froude number for riprap shear failure. This goal was adressed during the first four years of the project and resulted in two new two-parameter design formulas for riprap size selection for wing-wall and spill-through abutments placed in straight or curved compound channels.

The Year 5 reports investigates how the bed shear stress distributions over the riprap apron protecting wing-wall and spill-through abutments placed in a straight compound channel vary with increasing flow depth. As the flow depth increases, the flow at the bridge site transitions fom the free-surface (FS) flow regime to the pressurized flow (submerged orifice, SO or overtopping, OT) regime. This data is critical to propose corrections to existing design formulas for riprap size selection that were developed only the free surface regime such that estimates of the critical Froude number for riprap shear failure can be provided for cases when the bridge deck becomes submerged at high flow conditions.

Chapter 1 Introduction

1.1 Motivation and Proposed Approach

Maintaining roads operational requires reliable and safe transportation infrastructure design. This is especially the case for bridges that are river-crossing structures that need to remain operational during floods and other extreme weather events. Under high flow conditions, erosion occurs not only inside the main channel but also over its floodplains, especially in the region of flow contraction induced by the presence of bridge piers, bridge abutments and the attached embankments. Severe erosion problems were reported at many bridge sites, especially for abutments and embankments of smaller-size bridges. Severe scour can endanger the stability of the embankment and induce scour beneath the foundations of the abutments. In extreme cases, this may lead to bridge failure which results in interrupting the traffic and, in some cases, loss of human life. Two of the most encountered types of abutments used at bridges are spill-through and wing-wall abutments.

Considerable progress has been made over the two decades in understanding the mechanisms of local scour at abutments and in developing effective bridge-scour countermeasures to protect these structures against severe erosion (Sumer and Fredsoe 2002; Melville and Coleman 2000; Dey and Barbhuiya 2005; Kothyari at al. 2007; Sturm et al. 2011; Ettema et al. 2011, 2015, 2017; Koken and Constantinescu 2014; Hong and Abid 2019). One of the most popular and inexpensive ways to mitigate scour at bridge abutments is to use riprap stone to protect the river-bed regions situated next to these structures as well as the embankments of the abutments (Brown and Clyde 1989; Melville and Coleman 2000). The riprap stone provides an armor layer protection to the finer sediments present near the bed surface. When placed near the base of an abutment, the main effect of the apron is to modify the geometry of the scour hole such that the maximum scour

1

depth is reduced and the locations of large scour move away from the base of the abutment. To efficiently protect abutments against erosion (e.g., for design flood conditions at the bridge site), one needs to estimate the position and spatial extent of the region that needs to be protected and the minimum size (e.g., median diameter) of the riprap stone such that the stone will not be entrained by the overflow.

In general, the minimum size of the riprap stone in design equations is determined such that shear and edge failure are avoided (Chiew 1995; Melville et al. 2007; Barkdoll et al. 2007). Shear failure occurs where the individual riprap stones are not large enough to resist entrainment by the flow. The coefficients in the design equations for bridge abutments (Hoffmans and Verheij, 1997; Lagasse et al. 2001; Sumer and Fredsoe 2002; Melville and Coleman 2000; Melville et al., 2006a, 2006b; Cardoso et al. 2010) are mostly based on laboratory experiments conducted for a limited range of geometrical (e.g., straight channels, limited width of the floodplain or no floodplain) and flow conditions (open channel flow regime) at the bridge site. None of these design formulas can be used for cases when bank curvature effects are important or pressure scour effects due to bridge deck submergence are present. Laboratory experiments are very expensive to set up for cases when the bridge is situated in a region of significant channel curvature which probably explains the lack of design formulas that incorporate curvature effects.

Another general characteristic of most existing design formulas for bridge abutments is the minimum size of the median diameter of the riprap stone, D_{50}, in these formulas is only a function of the Froude number defined with the mean velocity in the contracted region containing the abutment and the flow depth. The effects of important geometrical parameters that affect the flow and its capacity to entrain sediment near bridge abutments (e.g., the floodplain width and the relative abutment length in the case of spill-through abutments, the floodplain width in the case of

spill-through abutments) are not accounted for in these formulas. Thus, there is a need to improve these guidelines and propose modified formulas or methodologies that can provide effective protection against erosion for a larger range of flow and geometrical conditions at these two types of abutments. The availability of more accurate and more general riprap-sizing design equations that can be effectively used in natural environments to protect bridge abutments and piers against erosion will result in a significant reduction of the risk of failure of bridges during natural disasters.

There is also a need to understand how the critical Froude number changes once the flow beneath the bridge deck becomes pressurized, which should lead to proposing corrections on how existing design formulas can be used to make predictions if the flow is pressurized at the bridge site. Such information is critical, as most of the local scour occurs at high flow conditions when the bridge deck becomes submerged.

One possible alternative to flume studies is to use numerical simulations to estimate the boundary shear stress over the channel bed, including over the regions protected by rock riprap. Correct estimation of the maximum bed shear stress over the regions protected by riprap stone requires accurate prediction of the velocity distribution near the abutment, where the flow is highly three dimensional. Fully 3-D, non-hydrostatic Reynolds-Averaged Navier-Stokes (RANS) models using two-equation turbulence closures are generally quite successful to predict flow and bed shear stress distributions in natural channels containing hydraulic structures (Roulund et al. 2005). Such models can account for the effect of the bed roughness on the flow and turbulence inside the channel (Zeng et al. 2008). For cases when the flow becomes pressurized at the bridge the free surface position is part of the solution and the rigid lid approach cannot be used. For such cases, the Volume of Fluid (VOF) method can be used to predict the free surface together with the flow field and bed shear stresses over the riprap apron.

If such a numerical approach is adopted, a series of 3-D simulations may be used to determine whether the riprap stone inside the apron will fail or not. For a given channel and abutment geometry, incoming flow discharge and flow depth, the predicted maximum shear stress over the riprap region is compared with the critical value for riprap failure to determine if the riprap stone will be entrained into the water column or not. To estimate the critical Froude number corresponding to the shear-failure entrainment threshold for the riprap stone, the discharge is then varied until the maximum bed shear stress over the riprap region is equal to the critical value. The procedure is the same for cases with free surface and pressurized flow regimes at the bridge site containing the abutments.

1.2 Prior Main Results and Findings

Figure 1.1 shows the general layout of the computational domain and the main geometrical variables (B_f=floodplain width, L_a=abutment length, y_m=flow depth over main channel, y_f=flow depth over the floodplains), as well as the position of the riprap apron. Outside of the riprap apron, the flat bed was covered with sand with d_{50}=0.82 mm. The inlet discharge was varied until the maximum value of the bed friction velocity over the riprap layer was $0.35u_{*cr}$, where u_{*cr} is obtained from the Shields diagram for a given mean diameter of the riprap stone, D_{50}. Following Melville and Coleman (2000), this value was used to determine the riprap shear failure entrainment threshold. The Froude number, Fr, was calculated using the mean velocity in the section containing the abutment.

The main research activity conducted during Year 1 was the validation of the method using the experimental data of Melville et al. (2007) for wing-wall abutments placed in a straight channel (Figure 1.1a). Simulations were conducted with flow only inside the main channel (y_m=0.1 m) and with flow over the floodplain (y_m=0.17 m, y_f=0.07 m) for B_f=0.4 m, 1.4 m, and 20 m and for 20

mm$<D_{50}<61$ mm. Five of the simulated test cases of the wing-wall abutment corresponded to those in the experiments of Melville et al. (2007). Figure 1.2 shows that for each of the five series of experiments, the numerically predicted shear failure entrainment threshold was situated in between the limiting experiments where no shear failure and shear failure, respectively, were observed.

During Year 2, a comprehensive parametric study was conducted for straight and curved channels containing wing-wall abutments at their two banks. The general layout is shown in Figure 1.3. Simulations were conducted for normal flow conditions (y_m=0.1 m) and with flow over the floodplains (y_m=0.17 m, y_f=0.07 m) and with varying riprap diameter (D_{50}=20 mm, 28 mm, 40 mm and 60 mm), floodplain width (B_f/W=0, 0.2 and 0.7), and channel radius of curvature (R/W=∞, 20, 10 and 1), where W=2 m is the width of the main channel. Using these data, the performance of existing design formulas (Pagan-Ortiz 1991; Lagasse et al. 2001) for riprap protection at bridges containing wing-wall abutments was checked for a wide range of conditions, outside of the range used to calibrate these formulas. A main finding was the two design formulas are not conservative enough for straight channels with a large floodplain width (Case III in Figure 1.4a). The design formulas were also found not to be conservative enough for cases where the abutments were placed in channels with a relatively high curvature ($R/W<20$).
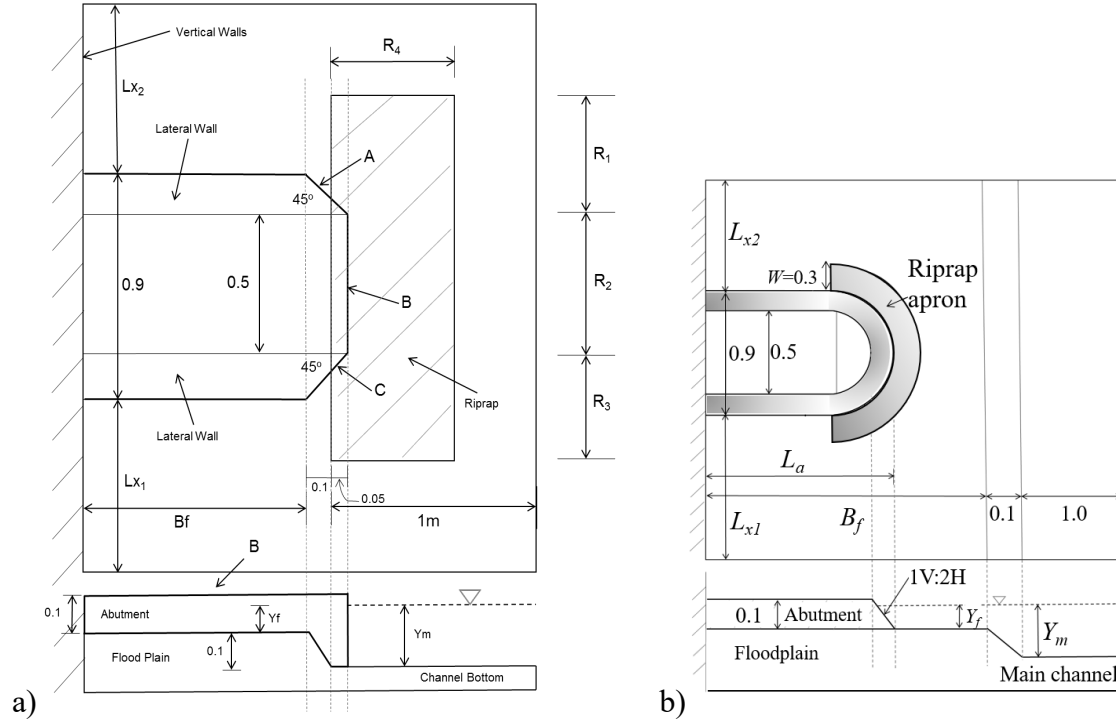
Figure 1.1 Sketch showing general layout of the preliminary numerical simulations performed for a wing-wall abutment (left) and for a spill-through abutment (right) placed on the floodplain of a straight channel. Dimensions are in meters. The wing-wall abutment geometrical set up corresponds to that used in the laboratory experiments of Melville et al. (2007). Reproduced from Wu et al. (2020) and Wu et al., (2021).
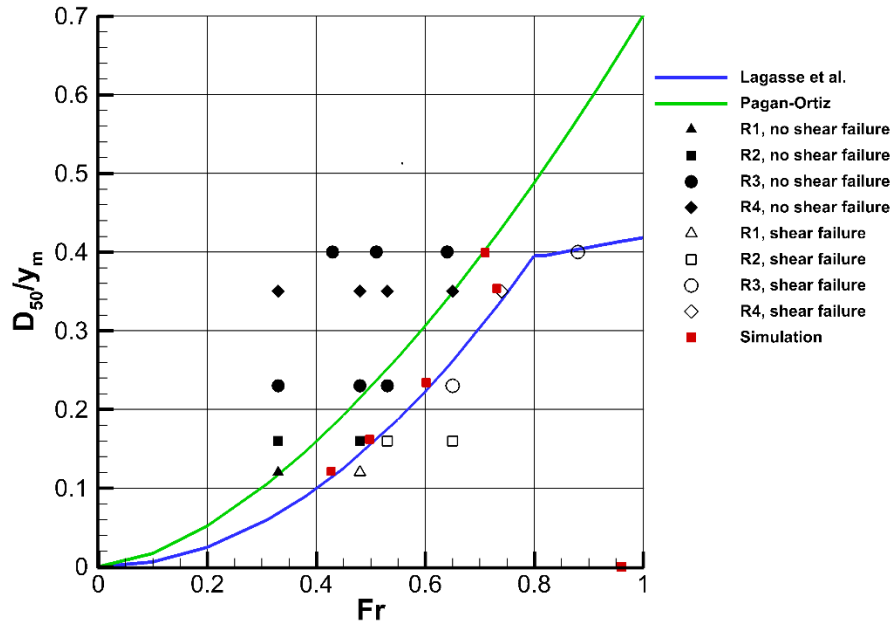
Figure 1.2 Validation of the numerical predictions of riprap shear failure for a wing-wall abutment placed in a straight channel. Also shown are predictions using the Lagasse et al. (2001) and Pagan-Ortiz (1991) equations and the experimental data of Melville et al. (2007). Simulation data (red squares) show predicted conditions for treshold of riprap entrainment by shear failure. Experimental data only show if shear failure occurred (open symbols) or not (solid symbols) in the corresponding experiments. Reproduced from Wu et al. (2020).
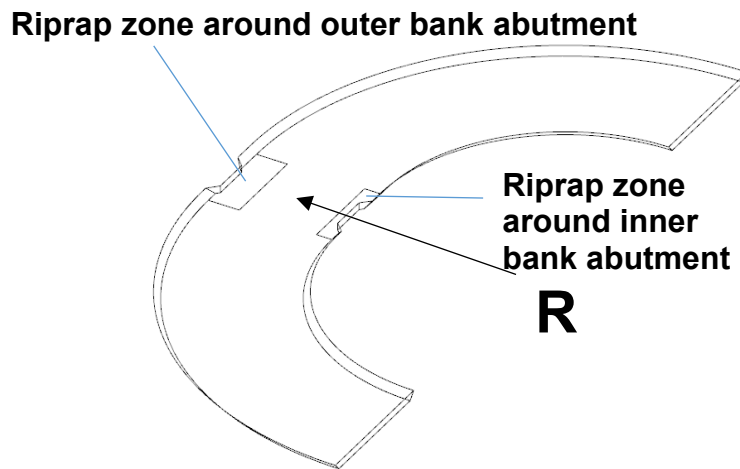
Figure 1.3 Sketch showing general layout used in the simulations performed in a curved channel containing an abutment at each bank. The channel radius of curvature is R.
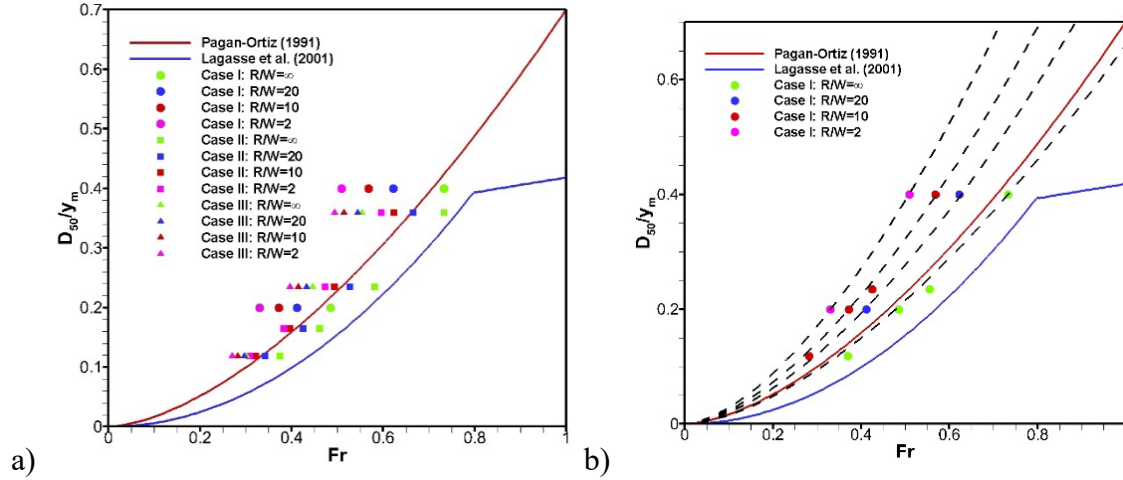
Figure 1.4 Comparison of numerical results with Lagasse et al. (2001) and Pagan-Ortiz (1991) equations for wing-wall abutments placed in straight and curved channels. The floodplain width is $B_f/W=0$ for Case I, $B_f/W=0.2$ for Case II and $B_f/W=0.7$ for Case III. Simulation data show predicted conditions for treshold of riprap entrainment by shear failure. The dashed lines in frame b show the new design formula predictions for Case I simulations. Partially reproduced from Wu et al. (2020).

The other main contribution of Year 2 was to propose a new design formula for wingwall abutments that retains the same functional relationship as that of Pagan-Ortiz (1991) and Lagasse et al. (2001) formulas:

$$D_{50}/y=(K_s/(S_s-1))^{0.5\alpha} *Fr^\alpha=C^{0.5\alpha}*Fr^\alpha \tag{1.1}$$

where K_s is the shape factor, $S_s=2.65$ is the specific gravity of the riprap stone, $C=K_s/(S_s-1)$ is a model coefficient and Fr is defined with the mean velocity in the section containing the abutments, V, and a characteristic length scale, y. For wing-wall abutments, $y=y_m$. Using this formulation, $C=0.645$ and $\alpha =1.62$ for the Pagan-Ortiz (1991) formula and $C=0.618$ and $\alpha =2.0$ for the Lagasse et al. (2001) formula (Fr<0.8). In the new design formula for wing-wall abutments, C and α are a function of the main nondimensional geometrical parameters (e.g., B_f/W, R/W). The

recommended values of C and α are summarized in Table 1.1. More details are given in Wu et al. (2020). One major finding was that α is not a function of the channel curvature, R/W, but increases monotonically with increasing B_f/W. The predicted range for α (1.62<α<1.84) was in between the values used by the Pagan-Ortiz (1991) formula (α=1.62) and Lagasse et al. (2001) formula (α=2).

Table 1.1 Best fit values of the power coefficient α and of the coefficient C as a function of the nondimensional radius of curvature R/H_{ref} and floodplain width, B_f/H_{ref} for a wing-wall abutment.

	$R/H_{ref}=\infty$	$R/H_{ref}=400$	$R/H_{ref}=200$	$R/H_{ref}=40$
	$R/W=\infty$	$R/W=20$	$R/W=10$	$R/W=2$
$B_f/H_{ref}=0.0$ $B_f/W=0$	α=1.62 C=0.60	α=1.62 C=0.82	α=1.62 C=0.99	α=1.62 C=1.25
$B_f/H_{ref}=4.0$ $B_f/W=0.2$	α=1.67 C=0.54	α=1.67 C=0.65	α=1.67 C=0.75	α=1.67 C=0.81
$B_f/H_{ref}=14.0$ $B_f/W=0.7$	α=1.84 C=1.07	α=1.84 C=1.11	α=1.84 C=1.24	α=1.84 C=1.32

The main contribution of Year 3 was to propose a new design formula for spill-through abutments positioned on the floodplain of straight channels. This new formula also assumes the form of eqn. (1.1) and its two coefficients are a function of the nondimensional abutment length L_a/B_f, and the floodplain width, B_f/H_{ref}. For spill-through abutments, Lagasse et al. (2001) formula for Fr<0.8 corresponds to C=0.54 and α=2 in eqn. (1.1) while Pagan-Ortiz (1991) formula corresponds to C=0.324 and α=2.
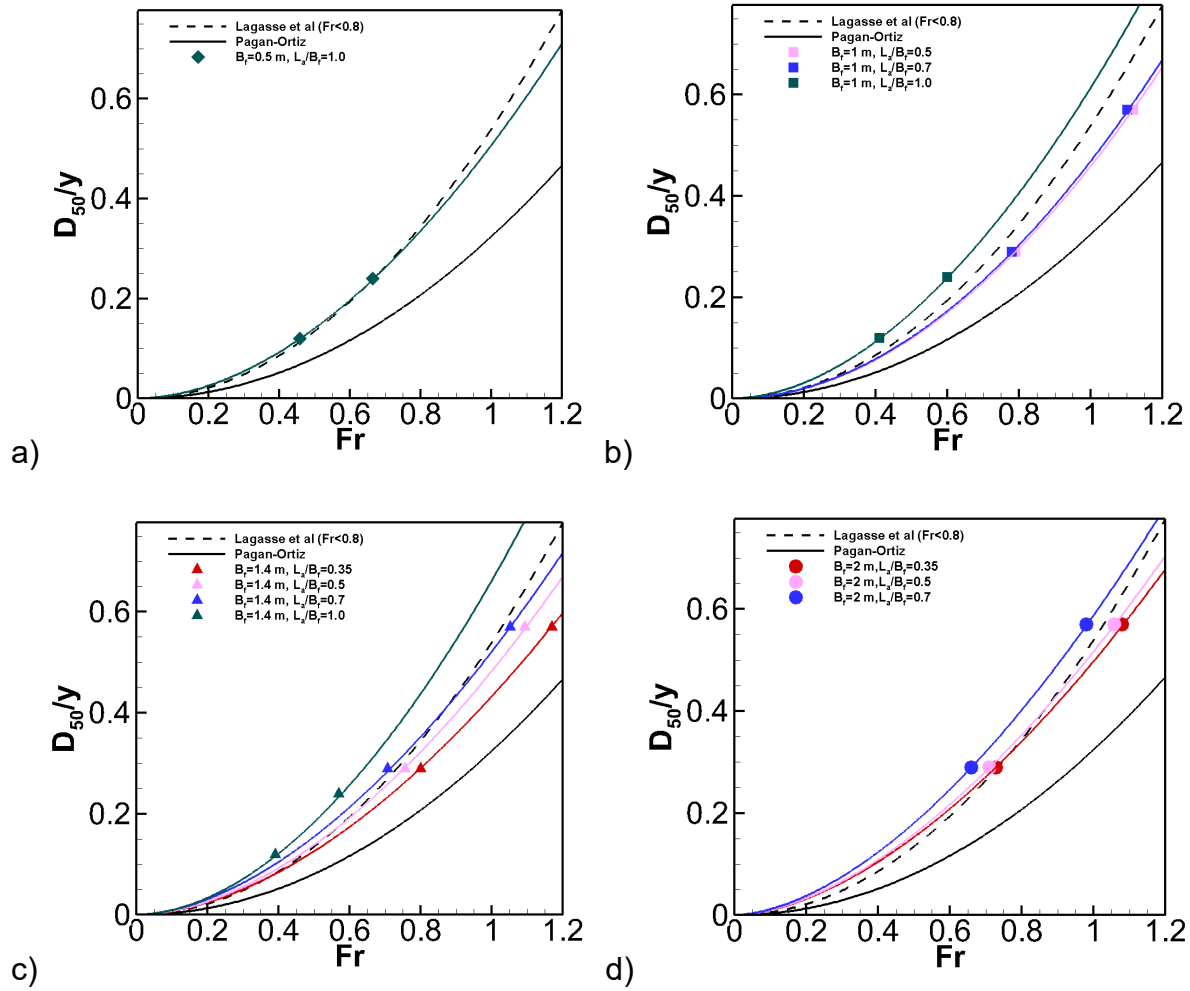
Figure 1.5 Comparison between the numerical predictions of the critical Froude number and Lagasse et al. (2001) and Pagán-Ortiz (1991) equations for spill-through abutments in a straightchannel. a) $B_f/H_{ref}=5$; b) $B_f/H_{ref}=10$; c) $B_f/H_{ref}=14$; d) $B_f/H_{ref}=20$. The colored lines show eqn. (1.1) predictions of the critical Froude number using best fit values of C and α.

Results in Figure 1.5 show that the Pagan-Ortiz formula is not conservative enough for all cases. The Lagasse et al. (2001) formula does much better; however, it still overpredicts the critical Froude number for cases with relatively large L_a/B_f. Its performance is much better for low B_f values (e.g., the formula is conservative enough for B_f=0.5 m). Results in Figure 1.5 also show that for constant D_{50}/y, Fr increases monotonically with decreasign L_a/B_f, an effect not captured by existing design formulas. Another interesting result is that α=1.85 for all cases with L_a/B_f=1

10

(abutment ressembles a wing-wall abutment) with C increasing with increasing B_f. For $0.3<L_a/B_f<0.8$, α is independent of L_a/B_f and C increases with increasing L_a/B_f. The predicted range of α was 1.7-1.95, slightly lower than the value, $\alpha=2$, in the Lagasse et al. and Pagan-Ortiz formulas.

A main contribution of Year 4 was to extend the design formula developed during Year 3 for cases when the spill-through abutment is placed in a curved channel with radius of curvature R. Details on the matrix of simulations used to develop a procedure to select the coefficients α and C for such cases is given in Wu et al. (2021). Tables 1.2 and 1.3 summarize the values of the two model parameters that need to be employed for cases when the abutment length is smaller than the floodplain width and when the abutment length is equal to the floodplain width, respectively. These tables allow estimating the model coefficients for practical cases using interpolation. For straight channels or for channels of very low curvature ($R/B_m > 100$), one should use the data for $R/B_m = 100$ in Tables 1.2 and 1.3 to determine the values of the model parameters. For $L_a/B_f < 1$, the interpolation should be first be done for L_a/B_f (only for C), then for B_f/B_m and, finally, for R/B_m (only C).

Table 1.2 Model parameters α and C in eqn. (1.1) for spill-through abutments with $0.35 < L_a/B_f \leq 0.9$. For channels with $R/B_m < 100$, use values given for $R/B_m = 100$ (from W et al., 2020b).

	$B_f/B_m = 0.5$	$B_f/B_m = 0.7$	$B_f/B_m = 1.0$
$R/B_m = 100$			
$L_a/B_f = 0.35$		$\alpha = 1.80$ $C = 0.39$	$\alpha = 1.75$ $C = 0.45$
$L_a/B_f = 0.5$	$\alpha = 1.95$ $C = 0.45$	$\alpha = 1.80$ $C = 0.45$	$\alpha = 1.75$ $C = 0.47$
$L_a/B_f = 0.7$	$\alpha = 1.95$ $C = 0.46$	$\alpha = 1.80$ $C = 0.48$	$\alpha = 1.75$ $C = 0.55$
$L_a/B_f = 0.9$	$\alpha = 1.95$ $C = 0.47$	$\alpha = 1.80$ $C = 0.51$	$\alpha = 1.75$ $C = 0.63$
$R/B_m = 20$			
$L_a/B_f = 0.35$		$\alpha = 1.80$ $C = 0.42$	$\alpha = 1.75$ $C = 0.48$
$L_a/B_f = 0.5$	$\alpha = 1.95$ $C = 0.45$	$\alpha = 1.80$ $C = 0.46$	$\alpha = 1.75$ $C = 0.52$
$L_a/B_f = 0.7$	$\alpha = 1.95$ $C = 0.46$	$\alpha = 1.80$ $C = 0.51$	$\alpha = 1.75$ $C = 0.61$
$L_a/B_f = 0.9$	$\alpha = 1.95$ $C = 0.47$	$\alpha = 1.80$ $C = 0.56$	$\alpha = 1.75$ $C = 0.70$
$R/B_m = 10$			
$L_a/B_f = 0.35$		$\alpha = 1.80$ $C = 0.44$	$\alpha = 1.75$ $C = 0.51$
$L_a/B_f = 0.5$	$\alpha = 1.95$ $C = 0.46$	$\alpha = 1.80$ $C = 0.49$	$\alpha = 1.75$ $C = 0.56$
$L_a/B_f = 0.7$	$\alpha = 1.95$ $C = 0.46$	$\alpha = 1.80$ $C = 0.54$	$\alpha = 1.75$ $C = 0.64$
$L_a/B_f = 0.9$	$\alpha = 1.95$ $C = 0.46$	$\alpha = 1.80$ $C = 0.59$	$\alpha = 1.75$ $C = 0.72$

Table 1.3 Model parameter C in eqn. (1.1) for spill-through abutments with $L_a/B_f = 1$ for which $\alpha = 1.85$. For channels with $R/B_m < 100$, use values given for $R/B_m = 100$ (From Wu et al., 2021)

	$B_f/B_m = 0.25$	$B_f/B_m = 0.5$	$B_f/B_m = 0.7$	$B_f/B_m = 1.0$
$R/B_m = 100$	$C = 0.48$	$C = 0.59$	$C = 0.64$	$C = 0.69$
$R/B_m = 20$	$C = 0.55$	$C = 0.67$	$C = 0.69$	$C = 0.71$
$R/B_m = 10$	$C = 0.63$	$C = 0.71$	$C = 0.72$	$C = 0.73$
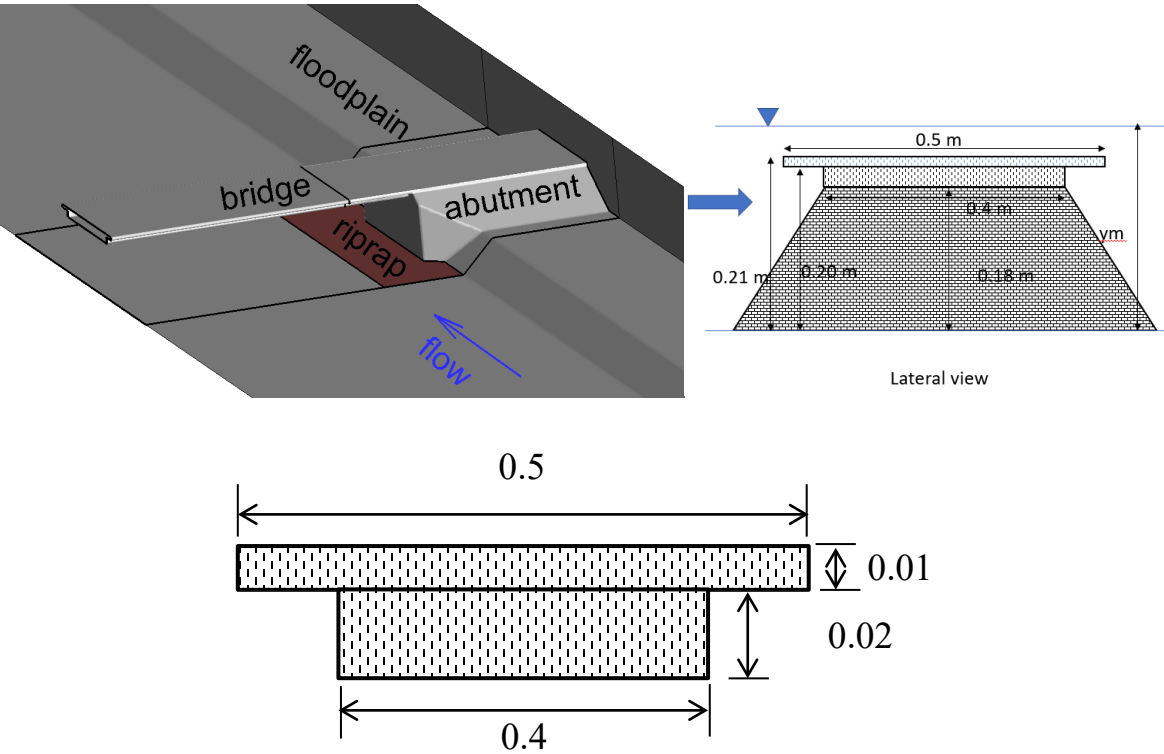
Figure 1.6 Sketch showing computational domain containign the wing-wall abutment and cross section cutting through the abutment and the bridge deck. Also shown in the bottom frame are the bridge deck and girders dimensions

The other major undertaking was to investigate how the critical Froude number varies with increased flow depth in the incoming channel as the flow regime changes from open channel to pressurized beneath the submerged bridge deck. This study is being conducted for wing-wall abutments placed in a straight channel (Figure 1.6). A major development was performing simulations with a deformable free surface using the Volume of Fluid method given that the rigid lid approximation is not valid anymore for pressurized flow simulations. The VOF module was validated and applied to estimate the critical channel discharge and the corresponding critical Froude number for different values of riprap size (28 mm<D_{50}<60 mm) and incoming flow depth in the main channel 0.17 m<y_m<0.24 m. Only preliminary simulations were performed in Year 4. Section 3 of the present report offers a full description of the simulations and results for wingwall abutments in a straight channel with pressurized flow regime at the bridge site.

1.3 Objectives

The main research objectives for Year 5 were to:

1.   Investigate how the flow, bed shear stress distributions, and the critical Froude number vary with increased flow depth in the incoming flow as the flow regime changes from free surface to pressurized beneath the deck of a bridge containing two wing-wall abutments placed in a straight compound channel. The investigation should be conducted with different flow depths in the approach flow and diameters of the riprap stone and should include cases when the bridge deck supported by the abutment is fully (overtopping regime) or partially submerged (orifice flow regime).

2.   Investigate how the flow, bed shear stress distributions, and the critical Froude number vary with increased flow depth in the incoming flow as the flow regime changes from free surface to pressurized beneath the deck of a bridge containing two spill-through abutments placed in a

14

straight compound channel. The investigation should be conducted with different flow depths in the approach flow and diameters of the riprap stone and should include cases when the bridge deck supported by the abutment is fully (overtopping regime) or partially submerged (orifice flow regime).

3.   Propose some simple recommendations on how to use existing design formulas for cases when the flow becomes pressurized at the bridge site.

<u>1.4 Justification of Research Approach</u>

Understanding and being able to quantitatively describe how the hydrodynamics of the stream flow field (velocity magnitude and bed shear stress distributions around the bridge site) changes with increasing stage and discharge as a result of a flood is critical to be able to propose effective measures to protect bridge abutments and piers against erosion. The National cooperative Highway Research Program Report 587 (NCHRP Report 587) used in the development of HEC 23 (2001, 2009) states the following:

> Selection of countermeasures to protect bridges from scour requires estimates of velocity distributions in the bridge opening. Estimates of the peak velocity in what is typically a highly non-uniform flow distribution near the tip of the abutment is necessary to determine whether countermeasures are necessary and, if so, to determine the type, size, and extent of countermeasures to protect bridge abutments from scour. Laboratory physical models have been developed to determine the size, type, and location of protection for a relatively small range of flow conditions at bridges; however, the laboratory models represent very simplistic geometric conditions. Effective transfer of laboratory model results to the complex hydrodynamic conditions of real bridge sites requires that flow velocity be predicted in the vicinity of bridge abutments using numerical models.

The report also comments on the limitations of the two-dimensional (2-D) depth-averaged modeling approach which was used in past studies to provide more accurate estimations of the variables in the design formulas used to protect against erosion. The main limitations of the 2-D approach are due to the hydrostatic pressure assumption and simplified turbulence modeling. Moreover, the region of maximum velocity amplification near the abutment toe is generally

located in a region of high flow curvature where 2-D numerical models are not very accurate. This is why the proposed approach is based on a fully three-dimensional approach.

The present study uses non-hydrostatic RANS simulations performed on fine meshes to obtain the 3-D mean velocity flow field. This allows direct estimation of the mean boundary shear stress over the whole bed region, including over the riprap apron. For cases when the flow becomes pressurized near the bridge, Volume of Fluid (VOF) RANS simulations are performed due to the need to predict the free surface position as part of the solution.

Given the detailed information on the flow fields, turbulence and their effects on the bed shear stress distributions available from such 3-D simulations, the proposed approach can lead to extension of the range of geometrical and flow configurations for which design formulas can be applied (e.g., abutments placed inside or immediately downstream of curved channels, high flow conditions that lead to the bridge deck becoming submerged). For such cases, laboratory experiments are very expensive and the range of geometrical (e.g., channel aspect ratio, width of the floodplain) and flow parameters in these experiments are even more limited compared to the canonical case of an abutment placed in a straight channel. The numerically based approach adopted in the present study does not face these limitations. Moreover, the numerical approach can be applied for cases when the flow regime changes from free surface to pressurized at the bridge site, a fairly common situation during high flow events (floods) when the most severe local scour is generally observed near the bridge abutments.

Chapter 2 Numerical Method

STAR-CCM+ is a state-of-the-art commercial code developed by CD-Adapco which solves the fully 3-D non-hydrostatic Navier-Stokes equations together with the turbulence model equations. The solver uses the finite-volume method to integrate the governing equations and allows the use of unstructured meshes. The RANS turbulence model provides the value of the eddy viscosity. The governing continuity and momentum equations are:

$$\frac{\partial U_i}{\partial x_i} = 0 \qquad (2.1)$$

$$\frac{\partial U_i}{\partial t} + \frac{\partial (U_i U_k)}{\partial x_k} = -\frac{1}{\rho}\frac{\partial P}{\partial x_i} + \frac{1}{\rho}\frac{\partial}{\partial x_k}\left[\left(\mu + \mu_t\right)\left(\frac{\partial U_i}{\partial x_k} + \frac{\partial U_k}{\partial x_i}\right)\right] - g\hat{k} \qquad (2.2)$$

where

U_i = Reynolds Averaged velocity component along the i direction

ρ = fluid density

μ = molecular dynamic viscosity

μ_t = eddy viscosity calculated from the RANS turbulence model

P = pressure

g = gravitational acceleration

$\hat{k}$ = unit normal vector along the vertical direction

The discretised Navier-Stokes equations are solved using a fractional-step algorithm. The advective terms are discretised using the second-order accurate upwind scheme, while the transient term discretization in time is second-order accurate based on an implicit representation. The

diffusive terms and the pressure gradient terms are discretised using the second-order accurate central scheme. The pressure-coupling is achieved using the SIMPLE algorithm. In the SIMPLE algorithm, the momentum equations without the pressure gradient term are advanced in time and an intermediate velocity is obtained which does not satisfy the continuity equation. A pressure-correction algorithm is then employed to modify the pressure field such that mass conservation is achieved.

Several two-equation turbulence models available in STAR-CCM+ were initially considered. The k-w SST model performed more accurately for channel flow simulations with a large value of the relative bed roughness, leading to its use in the simulations reported in this paper. STAR-CCM+ with the k-w SST turbulence model was widely used and validated for predictions of flow in channels containing hydraulic structures (Cheng et al. 2018), including for cases when an unsteady flood wave advanced in a channel with natural bathymetry (Cheng et al. 2018; Horna-Munoz and Constantinescu 2018, 2020).

For simulations with a deformable free surface, the Volume-of-Fluid (VOF) method is used to track the location of the free surface. A layer of air is present over the parts of the domain that contain, or can contain, water during the simulation. The VOF method is based on the advection of the volume fraction of water, α, for which a standard advection equation ($\frac{\partial \alpha}{\partial t} + U_j \frac{\partial \alpha}{\partial x_j} = 0$) is solved. In cells fully occupied by water $\alpha=1$, while in cells containing only air $\alpha=0$. The advection term in the VOF equation is discretised using the second-order upwind scheme. The temporal discretization is second order accurate.

No-slip boundary conditions were specified at all wall boundaries. The bed shear was calculated using the law of the wall for rough surfaces. At the rough-wall boundaries, the specified value of the surface roughness k_s was different over the riprap region ($k_s=D_{50}$) and over the rest of

the channel bed that was assumed to be covered by a layer of sand ($k_s=d_{50}$). The bed shear stress is estimated using the law of the wall for rough surfaces.

Preliminary straight and curved channel flow and steady RANS simulations with periodic boundary conditions in the streamwise direction were performed to obtain a fully developed channel flow solution to be used to specify the inlet boundary condition in the corresponding simulations of flow in compound channels containing an abutment on each floodplain. The cross section of the channel used in the preliminary simulations was identical to the inlet section of the computational domain in the simulations where abutments were present. The 2-D distributions of the velocity and the turbulence variables from the periodic simulations were specified at the inlet of the domain containing the abutments.

In the simulations performed with a rigid lid at the free surface, the outlet was specified as a pressure outlet boundary. Given the low value of the channel Froude number, the free surface was treated as a slip (symmetry) boundary on which the vertical velocity was set equal to zero. All simulations were performed in domains containing abutments at both sides of the channel. This is needed because in the case of curved channels the flow field is not symmetrical with respect to the axis of the main channel. The compound channel cross section was symmetrical with respect to the centerline of the main channel and the abutments placed over the two floodplains were identical.

In the VOF simulations, the height of the computational domain was larger than the flow depth inside the channel to allow for a layer of air to be present. The outlet and top (opened to air) boundaries were specified as pressure outlets. The desired pressure and volume fraction of water were directly specified on all outlet and top boundary surfaces. Specifying the distribution of the volume fraction of water is equivalent to imposing a free surface elevation at the outlet boundary. In the case when air was present next to the outlet boundary or the top boundary, the pressure

outlet was set to zero Pascals, and the volume fraction of water was set to $\alpha=0$. The inlet was specified as a velocity inlet with a specified level of the free surface. As VOF simulations were performed only for abutments placed in a straight channel, the computational domain contained only one abutment and half of the channel. A symmetry boundary condition was used in the symmetry plane of the channel (lateral boundary of computational domain).

STAR-CCM+ contains a very powerful meshing capability in which an initial geometry can be imported and smoothed in such a way to improve computational efficiency without loss of critical information. Once the geometry has been processed, a volume mesh is created with the desired meshing model to obtain a high-quality mesh. The grid generator allows the use of various controls and the generation of fine meshes in different parts of the domain where flow resolution needs to be higher (e.g., near the solid surfaces to resolve the attached boundary layers), which is essential to generate a high-quality mesh. One of the main advantages of the grid generator in STAR-CCM+ is that it allows automatic grid refinement in critical regions situated around the abutments with a smooth transition to regions where the mesh is coarser.

Chapter 3 Effect of pressurized-flow conditions on bed shear stress distributions and critical

Froude number for riprap aprons protecting wing-wall abutments placed in a straight compound

channel

Several series of VOF simulations of flow in a straight channel containing wing-wall

abutments were carried out. The simulations (Table 3.1) were conducted with different flow depths

in the approach flow and diameters of the riprap stone for cases when the bridge deck supported

by the wing-wall abutments is fully (overtopping flow regime, OT) or partially submerged

(submerged orifice flow regime, SO). The goal of these simulations was to investigate how the

critical discharge and the critical Froude number corresponding to entrainment of riprap stone of

a certain size decrease with increasing water elevation upstream of the abutments. Simulations

were also conducted with the same incoming flow depths but without a bridge deck to be able to

quantify the effect of pressurized flow conditions beneath the bridge deck on the critical discharge

and critical Froude number corresponding to shear failure of the riprap stone.

Due to the symmetry of the problem, the computational domain contained only half of the

channel and one abutment (Figure 1.6). Simulations were conducted with a bridge deck of

thickness d_{bd}=0.01 m and width 0.5 m. The thickness of the region containing the bridge

beams/girders was d_{bb}=0.02 m and its width was 0.4 m. The distance between the channel bottom

and the bottom of the region containing the bridge beams was y_D=0.18 m. The width of the main

channel was W=2 m. The channel half width was 1 m. The floodplain width was B_f=0.4 m.

The abutment (Figure 1.6) was identical to the one used in rigid-lid simulations that were

used in Year 2 to obtain a new two-parameter design formula for riprap sizing at wing-wall

abutments. The abutment has a trapezoidal cross section and its extremity slightly penetrates into

the main channel. The slope of the sidewalls are 1V:2H and the bottom width of the abutment is

0.9 m. As discussed by Melville et al. (2007), this abutment is representative of a four-lane highway bridge at a scale close to 1:20.
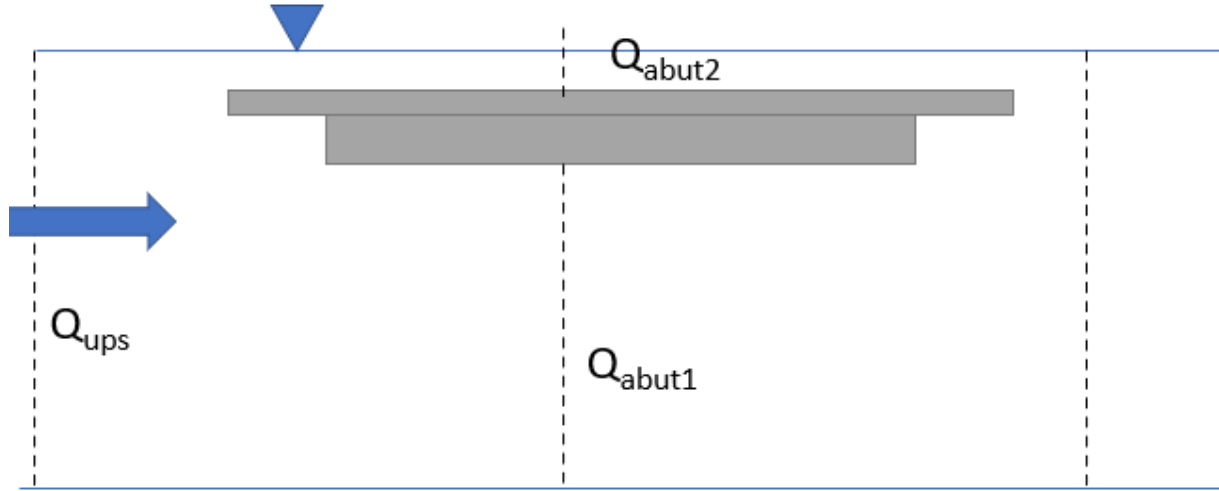
Figure 3.1 Sketch showing main flow variables for the case when the flow depth upstream of the abutment is sufficiently large for the bridge deck to become submerged. Part of the incoming flow (discharge Q_{ups}, mean velocity V_{ups}) is advected beneath the bridge deck (discharge Q_{abut1}, mean velocity V_{abut1}), the other part is advected over the bridge deck (discharge Q_{abut2}, mean velocity V_{abut2}).

Simulations in channels containing wing-wall abutments at their sides were performed with the same value of the mean sand diameter (d_{50}=0.00082 m) but with different values of the mean riprap stone diameter, D_{50}=0.061 m, 0.04 m, and 0.028 m. The total streamwise length of the riprap apron was 1.35 m, with riprap stone being present starting 0.5 m upstream of the abutment and ending 0.35 m downstream of it. The width of the riprap apron protecting the outer-bank abutment was 0.5 m. For each case, simulations were performed with different values of the inlet discharge until the maximum value of the bed friction velocity over the riprap region was equal to $u_{\tau c}$. This value is denoted Q_{upsc}. If the free surface reaches the bridge deck, then Q_{ups} has two components (Q_{abut1} and Q_{abut2}), as shown in Figure 3.1. The part of the total discharge, Q_{upsc}, advected beneath

the bridge deck at critical conditions is denoted Q_{abut1c}. A critical Froude number, Fr', can be defined with Q_{upsc} and y_{ups}, where y_{ups} is the constant flow depth upstream of the bridge deck. The men velocities in the incoming flow and beneath the bridge deck at critical conditions are denoted V_{upsc} and V_{abut1c} , respectively.

The VOF module was validated during Year 4 and then applied to estimate the critical channel discharge and the corresponding critical Froude number for different values of riprap size (0.028 m<D_{50}<0.06 m) and incoming flow depth in the main channel 0.17 m<y_m<0.24 m. The matrix of simulations is given in Table 3.1. The numerically predicted critical total discharge and the discharge beneath the bridge deck at critical conditions are given in Table 3.2. The same table shows the critical Froude number, Fr', for each case.

Table 3.1 Matrix of test cases for flow in a straight channel with a bridge containing two wing-wall abutments.

Case	Pressure flow types	Main-channel initial depth y_m (m)	Floodplain initial depth y_f (m)	Riprap stone size D_{50} (m)
Group 1 With bridge deck $(\tau_{max} = \tau_c)$	Free surface (FS)	0.17	0.07	0.028
				0.04
				0.061
	Submerged orifice (SO)	0.195	0.095	0.028
				0.04
				0.061
	SO~OT	0.205	0.105	0.028
				0.04
				0.061
	Overtopping (OT)	0.22	0.12	0.028
				0.04
				0.061
	Overtopping (OT)	0.24	0.14	0.028
				0.04
				0.061
Group 2 No bridge deck $(\tau_{max} = \tau_c)$	Submerged orifice (SO)	0.195	0.095	0.028
				0.04
				0.061
	SO~OT	0.205	0.105	0.028
				0.04
				0.061
	Overtopping (OT)	0.22	0.12	0.028
				0.04
				0.061
	Overtopping (OT)	0.24	0.14	0.028
				0.04
				0.061
Group 3 No bridge deck (use Q_c from group 1)	Submerged orifice (SO)	0.195	0.095	0.028
				0.04
				0.061
	SO~OT	0.205	0.105	0.028
				0.04
				0.061
	Overtopping (OT)	0.22	0.12	0.028
				0.04
				0.061
	Overtopping (OT)	0.24	0.14	0.028
				0.04
				0.061

Table 3.2 Main parameters predicted at critical conditions in the simulations conducted with $0.17 \leq y_m \leq 0.24$ m and three different values of D_{50}. See also Figure 3.1.

y_m (m)	D_{50} (mm)	y_{ups} (m)	D_{50}/y_{ups} (-)	$u_{\tau c}$ (m/s)	$u_{\tau max}/u_{\tau c}$ (-)	Q_{upsc} (m³/s)	V_{upsc} (m/s)	Q_{abut1c} (m³/s)	Q_{abut1c}/Q_{upsc} (-)	Fr'
0.17	28	0.17	0.165	0.058	1	0.088	0.406	0.088	1.00	0.432
0.17	40	0.18	0.222	0.07	1	0.100	0.446	0.101	1.01	0.491
0.17	61	0.18	0.339	0.084	1	0.122	0.525	0.122	1.00	0.598
0.195	28	0.191	0.147	0.058	1	0.094	0.380	0.081	0.86	0.391
0.195	40	0.203	0.197	0.07	1	0.113	0.438	0.099	0.88	0.455
0.195	61	0.208	0.293	0.084	1	0.132	0.494	0.118	0.90	0.549
0.205	28	0.203	0.138	0.058	1	0.096	0.372	0.080	0.83	0.383
0.205	40	0.21	0.190	0.07	1	0.115	0.428	0.100	0.87	0.429
0.205	61	0.216	0.282	0.084	1	0.142	0.535	0.124	0.87	0.531
0.22	28	0.221	0.127	0.058	1	0.096	0.331	0.073	0.76	0.311
0.22	40	0.228	0.175	0.07	1	0.122	0.423	0.099	0.81	0.413
0.22	61	0.234	0.261	0.084	1	0.150	0.508	0.129	0.86	0.516
0.24	28	0.24	0.117	0.058	1	0.105	0.303	0.077	0.73	0.305
0.24	40	0.252	0.159	0.07	1	0.148	0.448	0.109	0.74	0.422
0.24	61	0.258	0.236	0.084	1	0.173	0.519	0.132	0.76	0.510

Simulation results show that the main core of high streamwiswe velocity moves closer to the bed as the flow becomes pressurized (Figure 3.2) and the size of the region of relatively high bed shear stress over the riprap apron increases (e.g., it penetrates until the lateral edge of the riprap apron) as the flow accelerates beneath the bridge deck. Free surface effects are particularly strong in the y_m=0.24 m simulation (OT case) shown in Figure 3.2b. As expected, some of the incoming flow moves over the top of the bridge deck. A standing wave is generated near the upstream edge of the bridge deck and the free surface waviness is significant for a streamwise distance of about 3-4 times the width of the bridge deck. Over the bridge deck and downstream of it, the streamwise velocity is relatively high near the free surface. This effect increases monotonically with decreasing D_{50}.
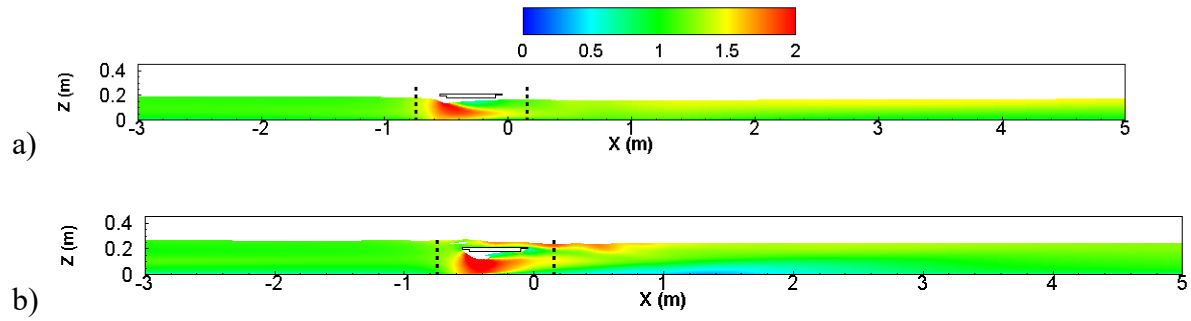
Figure 3.2 Normalized streamwise velocity distribution in a streamwise-vertical cross section situated close to the tip of the wing-wall abutment. Riprap size is D_{50}=0.061 m and B_f=0.4 m. a) free surface flow regime y_m=0.17 m; b) pressurized flow (overtopping regime) regime, y_m=0.24 m.
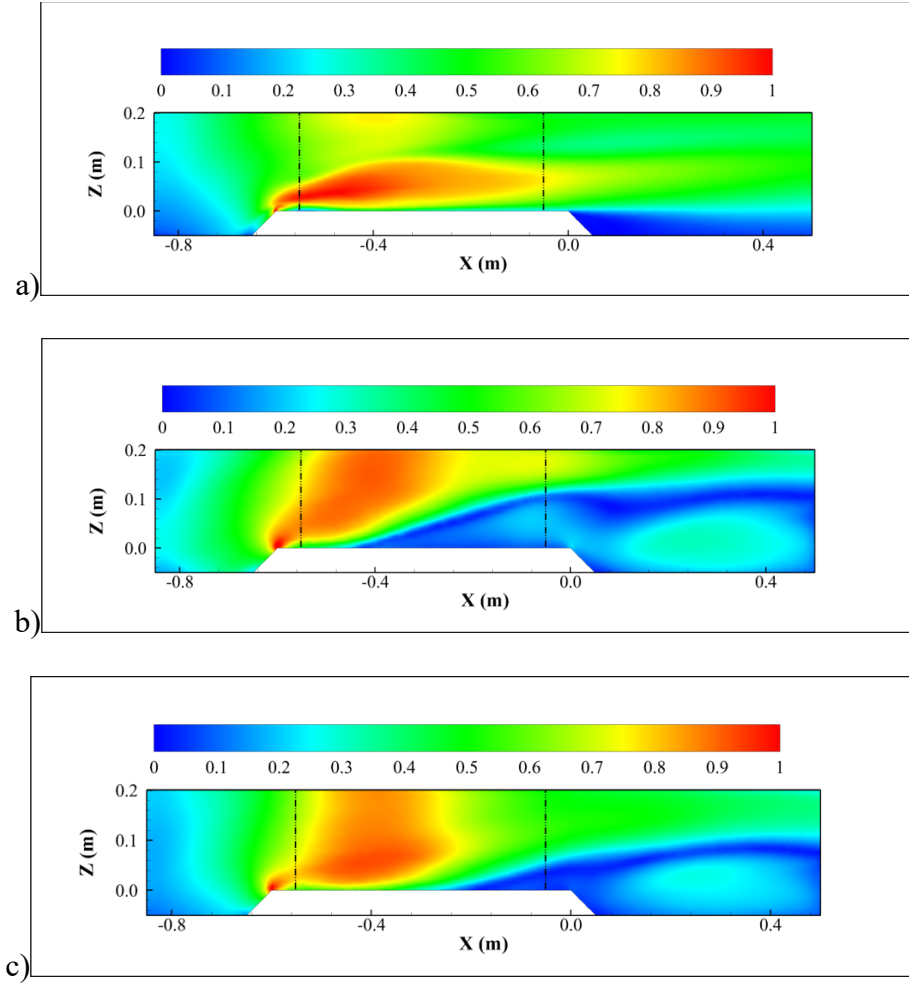
Figure 3.3 Normalized bed shear stress, τ/τ_{max}, over the riprap region at critical entrainment conditions when $\tau_{max}=\tau_{cr}$ (D_{50}=0.04 m, B_f=0.4 m). a) free surface flow regime, y_m=0.17 m; b) orrifice flow regime, y_m=0.195 m; c) overtopping flow regime, y_m=0.24 m.

The main effect of the flow becoming pressurized at the bridge site on the bed shear distributions over the riprap apron is an increase of the size of the region where the bed shear stress is close to the critical value. While in the FS regime, the high bed shear stress are confined to an elongated region close to the toe of the abutment (e.g., see Figure 3.3a), the region of high bed shear stress enlarges as the flow becomes pressurized (e.g., see Figure 3.3b for the OF regime and Figure 3.3c for the OT regime). This is due not so much to the reduction of the cross section because of the presence of the abutment but to formation of the core of high velocities present in

between the main channel bed and the bottom of the bridge deck. The region of relatively high bed

shear stress over the riprap apron extends until the lateral extremity of the apron in the pressurized

flow cases. In the cases where the flow is in the OF or OT regimes, the bed shear stress values

induced over the apron beneath the bridge deck become comparable to those recorded near the

upstream corner of the toe of the abutment (Figure 3.3).   This explains why scour is very severe

beneath the bridge deck once the flow becomes pressurized at the bridge site.

Table 3.3 Main parameters predicted in the series of simulations (group 3, see Table 3.1) performed without a bridge deck and using the critical discharge from the corresponding simulation in which the flow was pressurized at the bridge site.

y_m (m)	D_{50} (mm)	y_{ups} (m)	D_{50}/y_{ups} (-)	$u_{\tau c}$ (m/s)	$u_{\tau max}/u_{\tau c}$ (-)	Q_{upsc} (m^3/s)
0.195	28	0.198	0.141	0.058	0.912	0.094
0.195	40	0.204	0.196	0.07	0.915	0.113
0.195	61	0.209	0.292	0.084	0.899	0.132
0.205	28	0.203	0.138	0.058	0.879	0.097
0.205	40	0.209	0.191	0.07	0.878	0.113
0.205	61	0.215	0.284	0.084	0.867	0.137
0.22	28	0.205	0.137	0.058	0.827	0..096
0.22	40	0.222	0.180	0.07	0.833	0.116
0.22	61	0.234	0.261	0.084	0.842	0.155
0.24	28	0.24	0.117	0.058	0.771	0.105
0.24	40	0.252	0.159	0.07	0.795	0.146
0.24	61	0.251	0.243	0.084	0.799	0.172
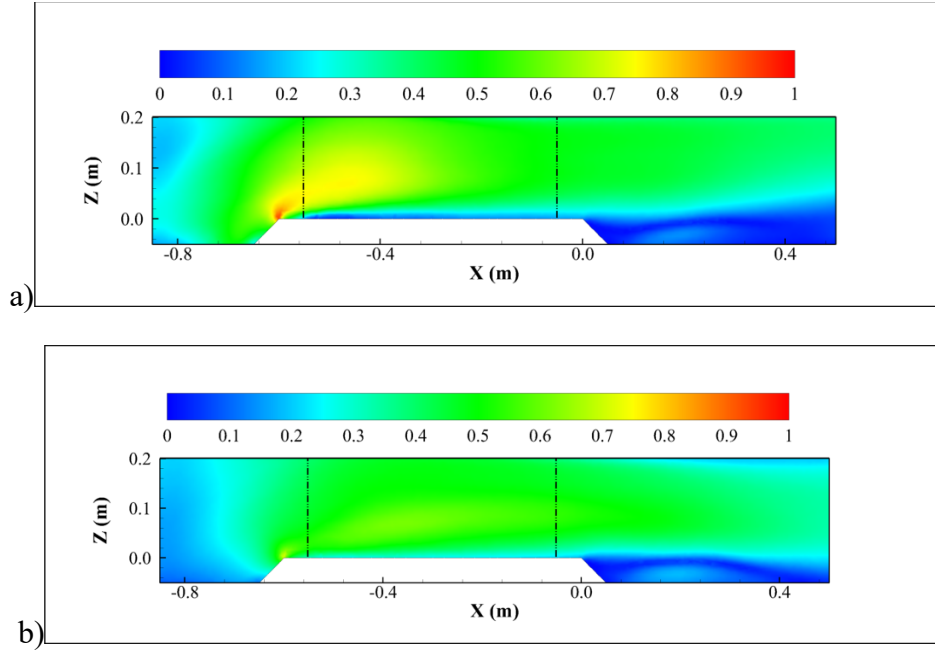
Figure 3.4 Normalized bed shear stress, τ/τ_{max}, over the riprap region for the case when the bridge deck is not present and the discharge Q is equal to the critical discharge calculated in the simulation with the bridge deck when the flow is pressurized at the bridge site (D_{50}=0.04 m, B_f=0.4 m). a) y_m=0.195 m; b) y_m=0.24 m.

To better understand the effect of the flow becoming pressurized in the simulations, additional simulations were conducted with the same value of y_m and the same value of the total incoming flow discharge at critical conditions but without a bridge deck. The matrix of these simulations is also given in Table 3.1 (group 3) and the main predicted variables are listed in Table 3.3. Comparison of the bed shear stress distributions in Figures 3.3b and 3.4a (y_m=0.195 m) and in Figures 3.3c and 3.4b (y_m =0.24 m) clearly show the peak bed shear stress and the average values of the bed shear stress over the riprap apron are lower in the free-surface simulations compared to the corresponding pressurized flow cases.

For y_m=0.24 m, the ratio between the peak bed shear stress over the riprap apron and the critical value for riprap entrainment varied between 0.77 and 0.8 in the simulations conducted with different values of D_{50} (Table 3.3). This shows that once the flow becomes pressurized, its capacity

to induce sediment entrainment increases significantly. For constant D_{50}, this ratio increases monotonically with decreasing y_m until it becomes equal to one when the flow at the bridge site transitions to the FS regime. In the present simulations, the distance between the bottom of the bridge deck and the main channel bed is $y_D=0.18$ m. For the OT regime, the maximum value of y_m/y_D is equal to 1.3 in the present series of simulations. For the SO regime, the maximum value of y_m/y_D is close to 1.15. Group 3 of simulations show up to 25% reduction of the maximum normalized bed friction velocity if y_0 and Q are the same but no bridge deck is present for the OT flow regime ($1.15<y_m/y_D<1.3$) and 15% maximum reduction for SO flow regime ($1<y_m/y_D<1.15$).

Simulations without a bridge deck were also conducted with the same values of y_m to determine the corresponding critical discharge (see group 2 simulations in Table 3.1). For example, for $y_m=0.24$ m, the ratio between the critical discharges in the corresponding simulations with no bridge deck and with bridge deck was 1.22 for $D_{50}=0.04$ m and 1.31 for $D_{50}=0.061$ m. Information on the values of the critical discharge and of the corresponding mean velocity at the abutment from the group 2 simulations can be used to propose an approximate way to account for the increased erosion potential for cases where the flow becomes pressurized at the bridge deck. The idea is to use the standard design formulas for the FS flow regime with same y_0 but with increased values of Q and velocity in the bridge section, V_{abut1}, compared to the actual values. For the SO regime ($1<y_m/y_D<1.15$), the maximum increase of Q is close to 15%. For the OT regime ($1.15<y_m/y_D<1.3$), the maximum increase of Q is close 40%. Evidently, this increase will be larger than 40% for $y_m/y_D>1.3$ but such cases are not very common. One should also point put that the aforementioned values were obtained for one channel geometry and one value of y_D. A more comprehensive parametric study is recommended to refine the multiplication factors for the discharge to be used in standard riprap sizing formulas.

Chapter 4 Effect of pressurized-flow conditions on bed shear stress distributions and critical Froude number for riprap aprons protecting spill-through abutments placed in a straight compound channel

Similar to the approach used in chapter 3 to investigate flow past wing-wall abutments in the FS, SO and OT regimes, several series of simulations with increasing flow depth in the incoming flow (y_m) were conducted with different values of the floodplain width, riprap diameter and relative abutment length, L_a/B_f, such that the flow regime changes from open channel to fully pressurized around the bridge site.

Simulations were conducted for three values of the incoming flow depth in the mean channel y_m=0.17 m (free surface, FS regime), 0.205 m (submerged orifice, SO regime) and 0.24 m (overtopping, OT regime), floodplain width B_f=1.4 m, main channel width, W=1.0 m, and abutment length L_a=0.5 m and 1.0 m. Simulations were conducted with two values of the mean riprap stone diameter, D_{50}=0.02 m and 0.04 m and a constant value of the mean sand diameter (d_{50}=0.00082 m). The matrix of simulations is given in Table 4.1. The bridge deck thickness and width are the same as those used for cases with wing-wall abutments. The spill-through abutment and the size of the riprap apron around it were identical to the ones in the rigid-lid simulations that were used in Year 4 to obtain a new two-parameter design formula for riprap sizing at spill-through abutments. The slope of the sidewalls are 1V:2H and the bottom width of the abutment is 0.9 m. As for the corresponding wing-wall abutment simulations, the distance between the main channel bed and the bottom of the bridge girders was y_d=0.18 m such that the flow is pressurized at the bridge site if $y_d<y_m$.

The computational domain around the bridge is shown in Figure 4.2 for one of the cases. Due to the symmetry of the problem, the computational domain contained only half of the channel

and one abutment. The mesh generation followed the same rules used for wing-wall abutments. Figure 4.3 shows the mesh on the main surfaces of the channel, bridge deck and spill-through abutment.

The main geometrical and predicted flow variables at critical conditions are summarized in Table 4.2. Based on the VOF predicted flow fields ($\alpha=1$ corresponds to water, $\alpha=0$ corresponds to air), the discharges are calculated using $Q = \int u\alpha dA$, and the mean velocities using $V = \frac{\int u\alpha dA}{\int \alpha dA}$. In each simulation, the incoming discharge Q_{ups} was varied until the maximum bed friction velocity over the riprap apron matched the critical value for sediment entrainment for the prescribed value of the riprap mean diameter, D_{50} (e.g., $u_{\tau max}/u_{\tau c}=1$). The value of the incoming discharge for these conditions is denoted Q_{upsc}. The subscript c is also us to denote the values of other variables at critical entrainment conditions over the riprap collar. If the free surface reaches the bridge deck, then Q_{ups} has two components (Q_{abut1} and Q_{abut2}), as shown in Figure 3.1. The corresponding mean velocities are V_{abut1} and V_{abut2}, respectively. A critical Froude number, Fr', can be defined with Q_{ups} and y_{ups}, where y_{ups} is the constant flow depth upstream of the bridge deck. For the pressurized cases y_{abut1} is the distance from the bottom of the main channel to the bottom of the girders. The values of the Froude number at critical conditions are also included in Table 4.2.
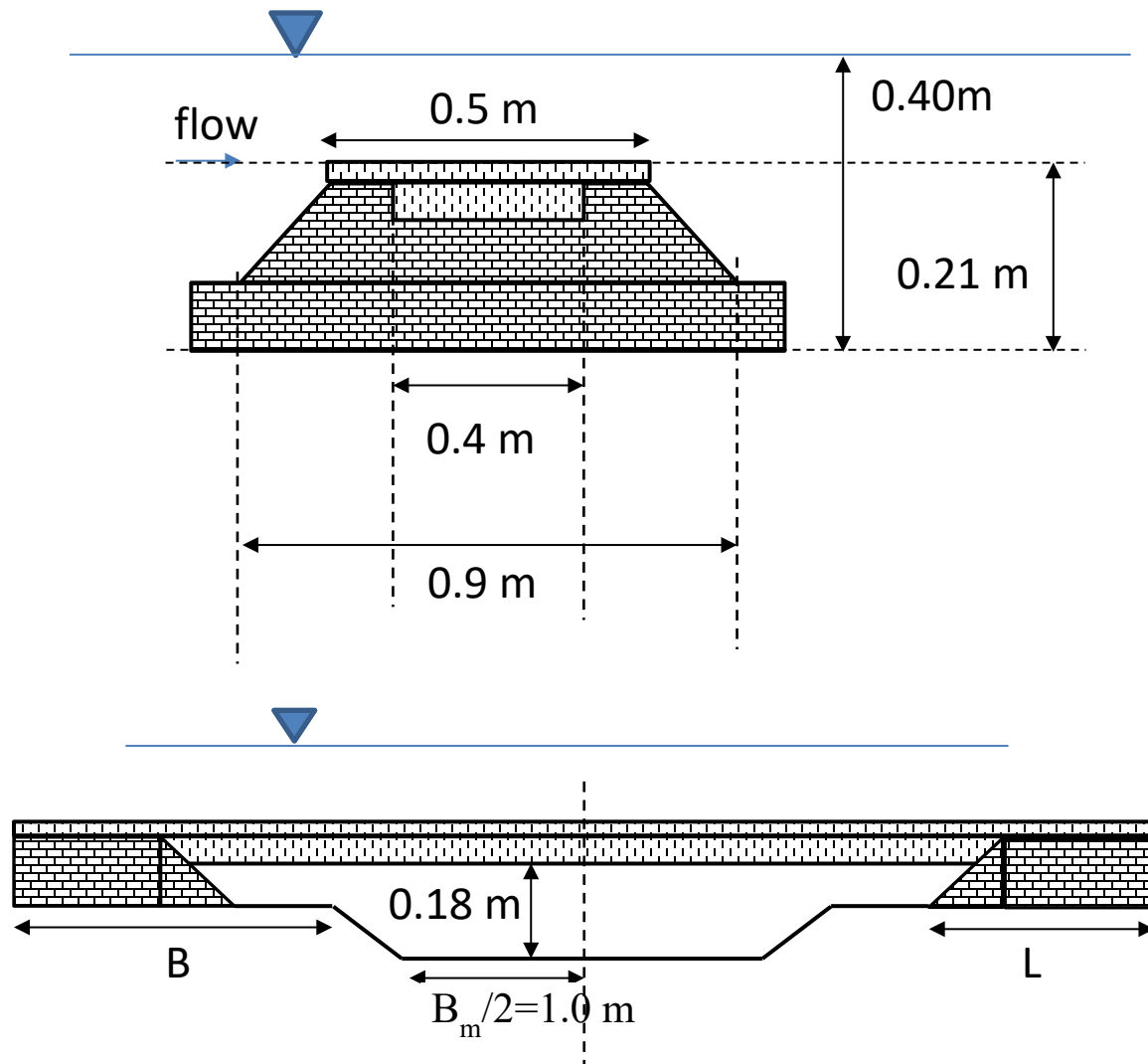
Figure 4.1 Setup of the simulations containing spill-through abutments in a compound channel with the bridge deck present. The two frames show a section of the abutment with the bridge deck and girders and a cross-section cutting through the symmetry plane of the abutments and bridge deck.
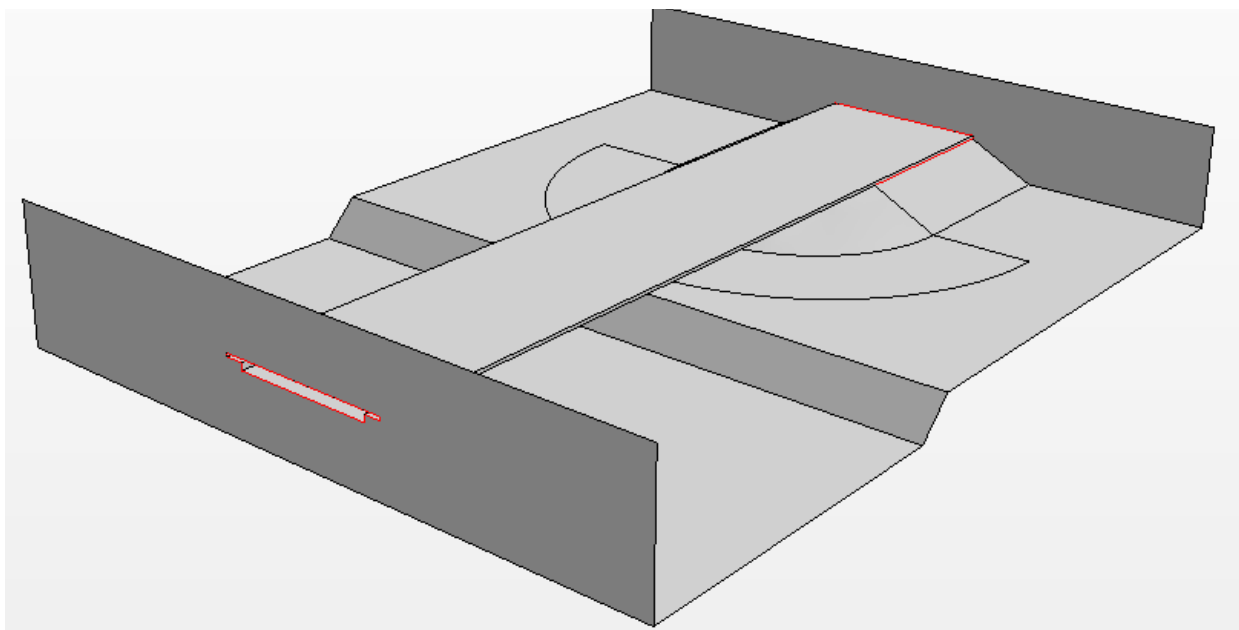
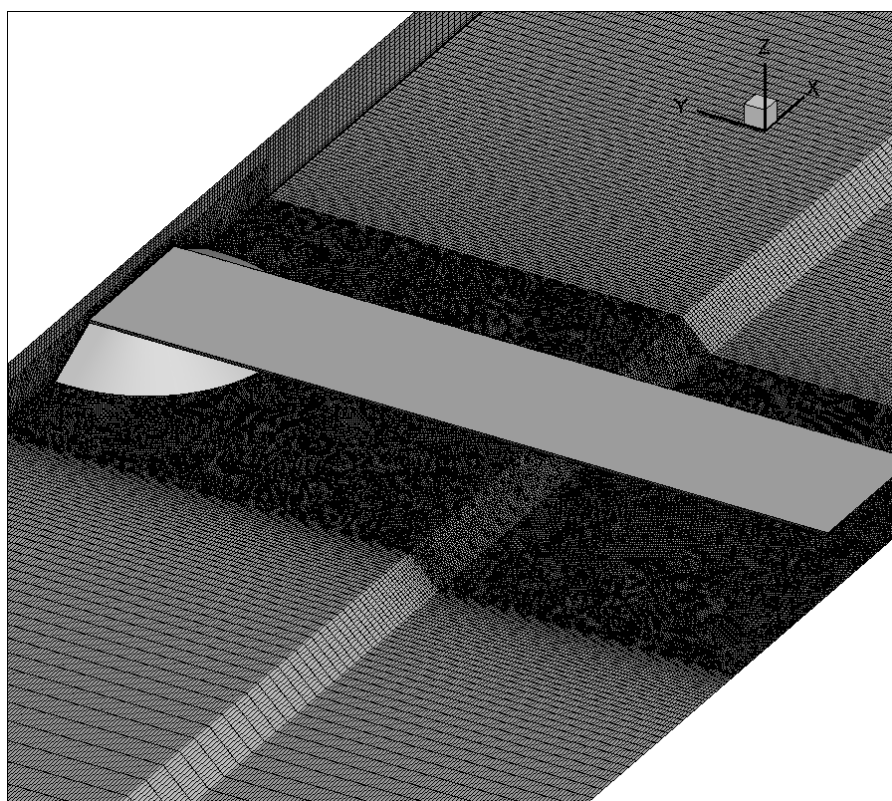**Figure 4.2** View of the computational domain in the vicinity of the bridge site

Figure 4.3 View of the computational mesh on the main surfaces.

34

Table 4.1 Matrix of test cases for flow in a straight channel with a bridge containing two spill-through abutments.

Pressure flow types	Main-channel initial depth y_m (m)	Floodplain initial depth y_f (m)	Abutment length L_a (m)	Riprap stone size D_{50} (m)
Free surface (FS)	0.17	0.07	0.5	0.02
				0.04
			1.0	0.02
				0.04
Submerged orifice (SO)	0.205	0.105	0.5	0.02
				0.04
			1.0	0.02
				0.04
Overtopping (OT)	0.24	0.14	0.5	0.02
				0.04
			1.0	0.02
				0.04

Table 4.2 Main parameters predicted at critical conditions in the simulations conducted with $0.17 \leq y_m \leq 0.24$ m and two different values of D_{50}.

y_m (m)	D_{50} (mm)	y_{ups} (m)	L_a (m)	D_{50}/y_{ups} (-)	$u_{\tau c}$ (m/s)	$u_{\tau max}/u_{\tau c}$ (-)	Q_{upsc} (m³/s)	Q_{abut1c} (m³/s)	Q_{abut1c}/Q_{upsc} (-)	V_{upsc} (m/s)	V_{abut1c} (m/s)	V_{abut1c}/V_{upsc} (-)	Fr_c'
0.17	20	0.170	0.5	0.118	0.048	1	0.109	0.109	1.00	0.36	0.42	1.16	0.328
0.17	40	0.175	0.5	0.229	0.07	1	0.153	0.153	1.00	0.46	0.57	1.24	0.436
0.205	20	0.200	0.5	0.100	0.048	1	0.109	0.108	0.99	0.29	0.40	1.40	0.286
0.205	40	0.205	0.5	0.195	0.07	1	0.163	0.155	0.95	0.40	0.57	1.42	0.403
0.24	20	0.234	0.5	0.085	0.048	1	0.139	0.109	0.79	0.31	0.40	1.30	0.266
0.24	40	0.234	0.5	0.171	0.07	1	0.196	0.152	0.77	0.40	0.56	1.39	0.369
0.17	20	0.171	1.0	0.117	0.048	1	0.109	0.108	1.00	0.34	0.48	1.41	0.372
0.17	40	0.182	1.0	0.220	0.07	1	0.152	0.151	1.00	0.42	0.66	1.56	0.488
0.205	20	0.200	1.0	0.100	0.048	1	0.112	0.109	0.97	0.29	0.48	1.65	0.341
0.205	40	0.210	1.0	0.190	0.07	1	0.180	0.161	0.89	0.41	0.67	1.61	0.467
0.24	20	0.233	1.0	0.086	0.048	1	0.142	0.109	0.76	0.30	0.47	1.57	0.310
0.24	40	0.248	1.0	0.161	0.07	1	0.225	0.163	0.72	0.44	0.68	1.55	0.435
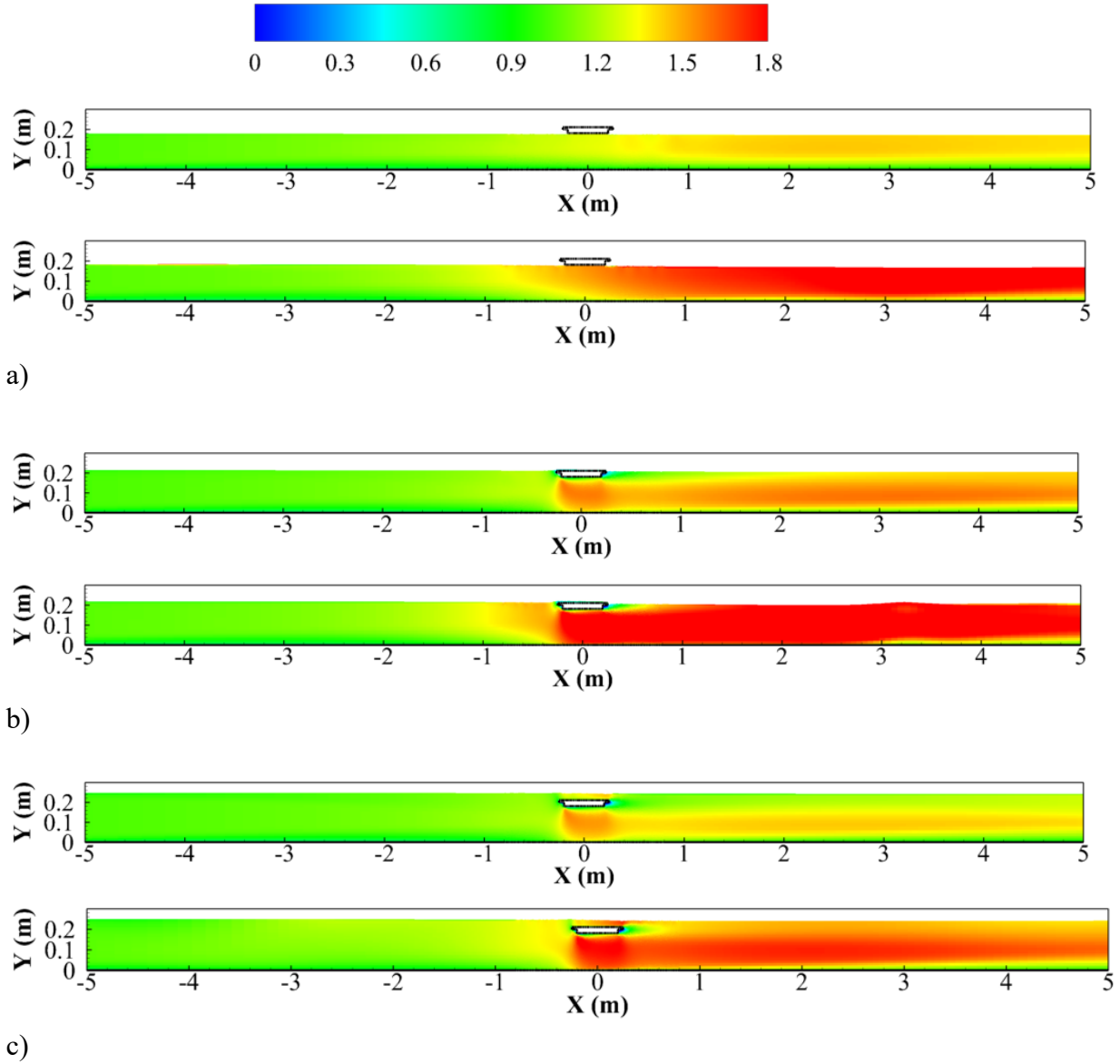
Figure 4.4 Normalized streamwise velocity distribution in a streamwise-vertical cross section situated close to the front edge of the spill-through abutment. Riprap diameter is D_{50}=0.020 m. The abutment length is L_a=0.5 m in the top figure of each frame and L_a=1.0 m in the bottom figure of each frame. a) open channel flow y_m=0.17 m; b) pressurized flow (submerge orifice regime), y_m=0.205 m; c) pressurized flow (overtopping regime), y_m=0.24 m.

The streamwise velocity magnitude distributions in a streamwise-vertical plane in figure 4.4 show a clear qualitative difference between the open channel flow cases (fig. 4.4a) and the pressurized flow cases (figs. 4.4a and 4.4b) for both values of the abutment length. A region of

high velocity magnitude forms beneath the bridge deck in the pressurized flow cases. Moreover, the core of high velocites moves closer to the channel bed. This is the main mechanisms responsible for the increase of the bed friction velocity due to the flow becoming pressurized at the bridge site. Though in the OT regime (Figure 4.4c), some of the incoming flow moves over the bridge deck, no large-scale oscillations of the free surface are observed downstream of the bridge as was the case in the corresponding simulations performed with a wing-wall abutment.

Figure 4.5 Normalized bed shear stress, τ/τ_{max}, over the riprap region at critical entrainment conditions where $\tau_{max}=\tau_{cr}$ in the simulations performed with spill-through abutments ($D_{50}=0.04$ m, $B_f=1.4$ m, $L_a=0.5$ m). a) free surface flow regime, $y_m=0.17$ m; b) orrifice flow regime, $y_m=0.205$ m; c) overtopping flow regime, $y_m=0.24$ m.

As opposed to what was observed for wing-wall abutments, the distribution of the normalized bed shear stress at critical conditions is qualitatively similar in the FS cases (Figures 4.5a and 4.6a) and the cases where the flow becomes pressurized (SO regime in Figures 4.5b and 4.6b and OT regime in Figures 4.5c and 4.6c). This is mostly because in the case of spill-through

abutments the apron is situated over the floodplain. In fact, the size of the region of relatively high values of the normalized bed shear stress slightly decays with increasing flow depth in the incoming flow. Of course, the critical conditions are reached at lower and lower values of Q_{ups} as the incoming flow depth increases.
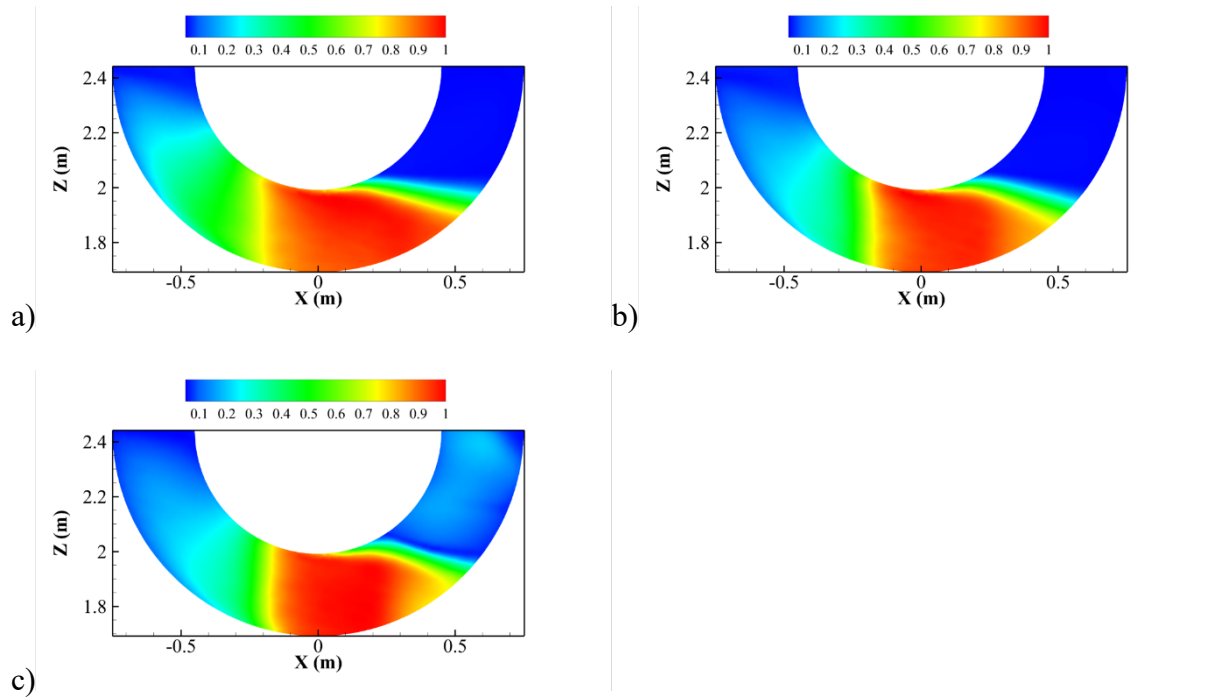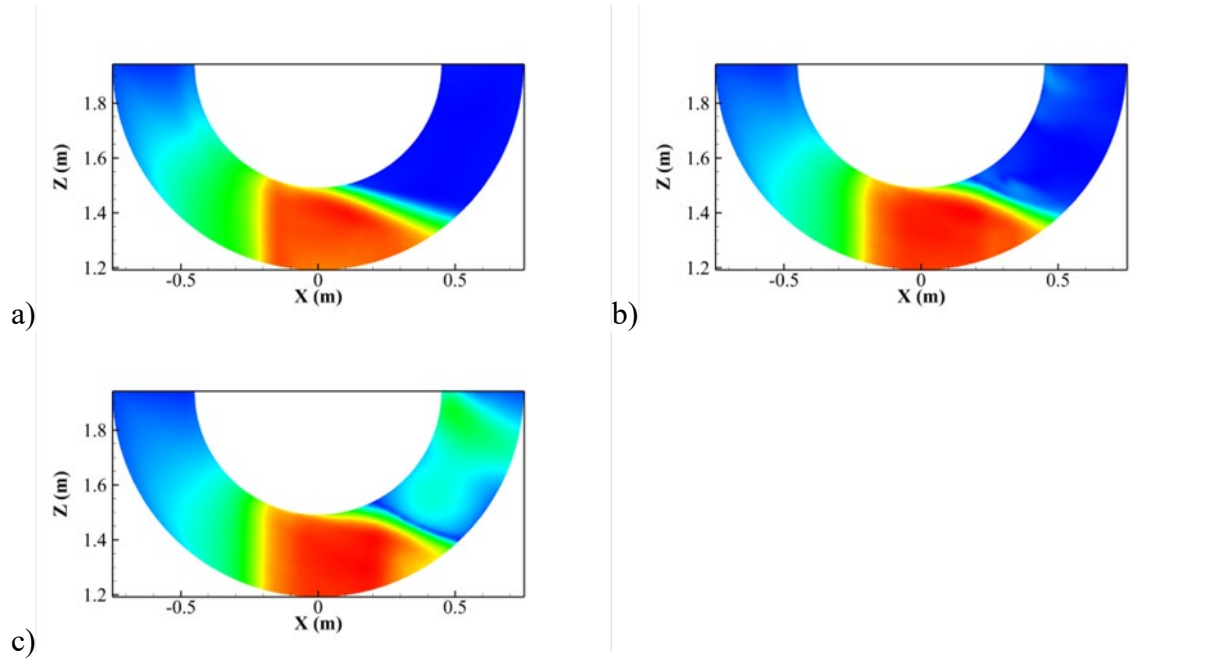

Figure 4.6 Normalized bed shear stress, τ/τ_{max}, over the riprap region at critical entrainment conditions where $\tau_{max}=\tau_{cr}$ in the simulations performed with spill-through abutments (D_{50}=0.04 m, B_f=1.4 m, L_a=1.0 m). a) free surface flow regime, y_m=0.17 m; b) orrifice flow regime, y_m=0.205 m; c) overtopping flow regime, y_m=0.24 m.

Figure 4.7 shows the variation of Fr' with the ratio between the sediment size and the upstream flow depth. In principle, the flow depth at the bridge site should be used for this type of plots. However, for practical applications only y_{ups} is known (Table 4.2) together with the distance between the bridge deck and the channel bed, y_d. Results in Figure 4.7 suggest that all points corresponding to the simulations with L_a=0.5 m can be plotted on only one curve $\frac{D_{50}}{y_{ups}} = C^{\alpha/2} Fr'^{\alpha}$ regardless of whether or not the flow is pressurized or not. The same is true for the simulations

conducted with $L_a=1.0$ m. The best fit values of the model coefficients are $C=1.2$ and $\alpha=2.0$ for $L_a=0.5$ m and $C=0.88$ and $\alpha=2.0$ for $L_a=1.0$ m. As expected, as y_{ups} increases, Fr' decreases for a constant riprap stone diameter, D_{50}.
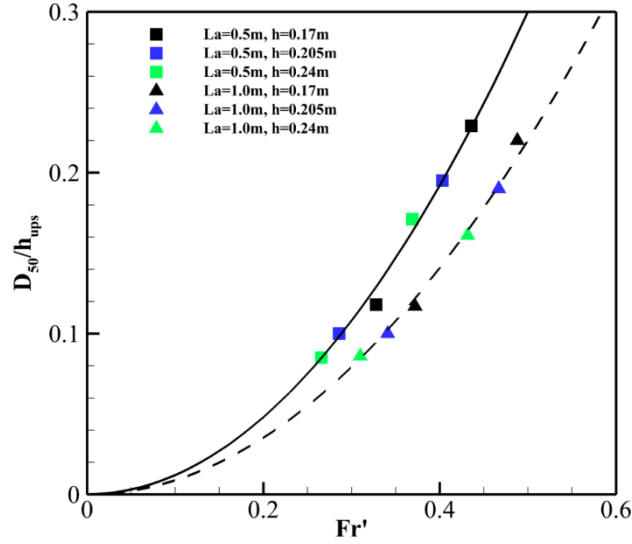
Figure 4.7 Nondimensional riprap stone size vs. critical Froude number, Fr' in the simulations performed with spill-through abutments. Results are shown for both $L_a=0.5$ m and $L_a=1.0$ m and different values of D_{50}.

Figure 4.8 shows how the ratio between the discharge moving beneath the bridge deck and the total incoming flow discharge starts decreasing once $y_{ups}>y_D$ in the simulations conducted with $L_a=0.5$ m and $L_a=1.0$ m. For same value of L_a, Q_{abut1}/Q_{ups} decreases with increasing D_{50}. For same value of D_{50} and y_{ups}, Q_{abut1}/Q_{ups} decreases with increasing L_a due to the larger constriction in the bridge section which further increases pressurized flow effects. As a result, a larger fraction of the incoming flow is diverted over the bridge deck. In the OT cases with $y_m=0.24$ m for which $y_m/y_D=1.3$, Q_{abut1}/Q_{ups} is close to 0.72 in the simulations conducted with $L_a=1.0$ m. So, more than a quarter of the incoming discharge moves over the bridge deck in this case. However, even though

a significant part of the incoming flow is not advected beneath the bridge deck, the erosion potential of the flow growth much faster with increasing y_0 in the pressurized flow cases compared to the corresponding free surface flow cases, when the bridge deck is absent.
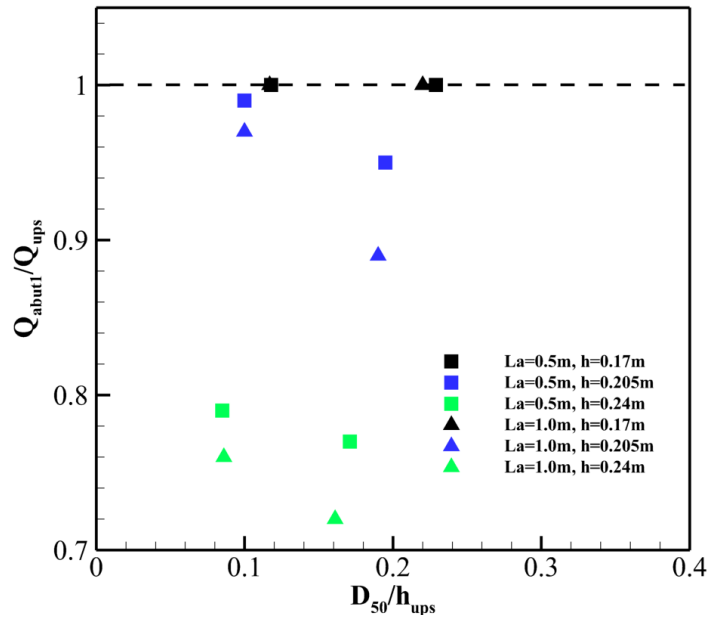

Figure 4.8 Ratio between the discharge passing under the bridge deck and the total channel discharge as a function of the abutment length and flow depth near the bridge site.

Chapter 5 Conclusions and Proposed Future Work

As part of the present research project, a general methodology based on fully 3-D, non-hydrostatic RANS numerical simulations was developed to determine the conditions for riprap shear failure for cases when a riprap apron is placed close to an abutment in a compound channel. The relationship proposed by Melville and Coleman (2000) and Melville et al. (2007) for riprap entrainment threshold (shear failure mode) was used to determine if riprap stone entrainment occurs. The methodology was validated during Year 1 for wing-wall abutments using the experimental data of Melville et al. (2007). Based on data obtained using this methodology, a new two-parameter riprap sizing design formula was proposed for wing-wall abutments in Year 2. The proposed numerical approach is much less expensive compared to the classical one based on laboratory scaled-model investigations and allows incorporating additional complexities present at many bridge sites.

A main finding of the study carried during Year 3 for spill-through abutments placed in a compound straight channel was the data generated via numerical simulations showed the Lagasse et al. (2001) formula gave more accurate predictions compared to the Pagan-Ortiz (1991) formula. Still, even the Lagasse et al. (2001) formula overpredicted the critical value of the Froude number for test cases conducted with high values of the floodplain width (e.g., B_f=2.0 m). Slight overpredictions were observed, even for smaller values of B_f, if the relative length of the abutment, L_a/B_f, was sufficiently large. The critical Froude number was found to decay monotonically with the decrease in L_a/B_f, an effect not accounted for in any existing design formulas.

The main outcome of the research performed during Year 4 was a new, two-parameter riprap sizing formula for protection of spill-through abutments against erosion. The formula can be used in both straight and curved compound channels with a radius of curvature of the main

channel, *R*, that is less than 10 times the channel width, B_m. This significantly enlarges the range of practical conditions where the new formula can be applied, as many bridges are built in regions where the channel curvature is not negligible. The formula retains the functional relationship ($D_{50}/y=C^{0.5\alpha}*Fr^{\alpha}$) of the Lagasse et al. (2001) and Pagan-Ortiz (1999) formulas used for riprap apron design at wing-wall and spill-through abutments. The present numerical predictions were able to understand the effects of the various geometrical parameters (e.g., floodplain width, channel radius of curvature, relative abutment length) on the critical Froude number needed to avoid shear failure of riprap stone of a given diameter. Standard design formulas do not incorporate the effects of all these variables on the critical value of the Froude number that will result in riprap entrainment. Increasing channel curvature was found to further reduce the critical Froude number at which riprap shear failure occurs at the outer-bank, spill-through abutment. So, to provide accurate predictions for such cases, the model parameters should also be a function of the radius of curvature of the channel, *R*. The new design formula was found to adequately fit all the data sets generated via numerical simulations.

The main outcome of Year 5 was to develop a new version of the 3-D RANS numerical model that can be used to predict bed shear stress distributions over the apron region for cases when the free surface elevation needs to be computed as part of the solution. This is needed to study cases when the free surface interacts with the bridge deck. Simulations with a deformable free surface using the Volume of Fluid method were performed given that the rigid lid approximation is no longer valid for pressurized flow simulations. Besides the abutment placed in a compound channel, the bridge deck was part of the computational domain.

Simulations conducted for wing-wall and spill-through abutments covered a wide range of relevant cases. With increased flow depth in the incoming flow, the flow regime near the bridge

deck connecting the abutments placed on the two floodplains changed from free surface (FS) flow regime to submerged orifice (SO) flow regime and then to (bridge-deck) overtopping (OT) flow regime. Simulations conducted with SO and OT flow regime at the bridge site were found to be characterized by very complex patterns of the velocity and bed shear stress distributions inside the pressurized-flow region and downstream of it. Simulation results showed that the core of high streamwiswe velocity moved closer to the bed as the flow became pressurized.

The numerical model was then used to predict how the critical Froude number and the critical discharge defined using the flow depth in the approaching flow varied as the elevation of the free surface increases. The main variables that were varied were the riprap stone diameter, the width of the floodplain and the relative length of the abutment in the case of spill-through abutments. Additional simulations performed without bridge deck for the same geometrical conditions and same water depth in the incoming flow as that in the corresponding pressuried flow cases. These additional simulations allowed determining the critical discharge that will be required to induce critical conditions for riprap entrainment assuming free surface flow regime at the bridge site. Based on analysing the ratio of these two discharges, some recommendations were made on how to determine the critical Froude number for OT and SO flow regimes using the standard design formulas proposed for FS flow regime. The idea is to use the same flow depth but larger discharges than the actual ones to estimate a modified critical Froude number. Then this Froude number can be used in standard design formulas proposed for the FS regime to determine the mimimum size of the riprap stone.

A main direction for future work will be to generate more data for abutments where the flow at the bridge site is pressurized (OT and SO regimes) such that new design equations can be proposed. The challenge is that the split of the incoming discharge into the two components

moving beneath and over the bridge deck is not known apriori. So, such new design formulas have to be based only on the discharge and flow depth in the approaching flow and on the distance between the channel bed and the bottom of the bridge deck.

We also recommend that the present numerically based approach should be applied for bridge piers, in particular for piers of circular and rectangular shapes which are the most common types of piers used at both small and large bridges. Presently, there are no design formulas that can be applied for cases when the flow is pressurized at the bridge site to determine the minimum diameter of the riprap stone needed to effectively protect the pier against scour. Multiparameter formulas can be proposed to design the riprap apron at bridge piers under a variety of flow and geometrical conditions.

We will work with the Transportation Research Board committee TRB-AFB60 such that the main findings and the proposed new design formulas for determining minimum riprap size at wing-wall and spill-through abutments will be considered for adoption in a future FHWA Technical Brief update to HEC 23. Once adopted, the new procedure will enhance the capabilities of state DOTs to develop more reliable approaches to protect bridges against possible failure induced by severe erosion associated with flood events. At a more general level, more accurate riprap design formulas for protection of abutments against erosion will result in significant reduction of the costs to operate roads during and after flood events. It will also contribute to reducing the risk for hazards associated with bridge failure during floods by avoiding structural failure.

References

Barkdoll, B. D., Ettema, R., & Melville, B. W. (2007). *Countermeasures to protect bridge abutments from scour* (NCHRP Project 24-18. NCHRP Report 587). Transportation Research Board.

Brown, S. A., & Clyde, E. S. (1989). *Design of riprap revetment: Hydraulic Engineering Circular No. 11* (FHWA-IP-016). National Highway Institute (US).

Cardoso, A., Simarro, G. and Schleiss, A. (2010). *Sizing of riprap for spill-through abutments, Water Management*, 163, issue WM10, 499-507, Paper 900024.

Cheng, Z., Koken, M. and Constantinescu, G. (2018). Approximate methodology to account for effects of coherent structures on sediment entrainment in RANS simulations with a movable bed and applications to pier scour. *Advances in Water Resources,* 120, 65-82.

Chiew, Y. M. (1995). Mechanics of riprap failure at bridge piers. *Journal of Hydraulic Engineering*, *121*(9), 635-643.

Dey, S. & Barbhuiya, A.K. (2005). Time variation of scour at abutments. *Journal of Hydraulic Engineering, 131(1),* 11-23.

Ettema, R, Constantinescu, G and Melville, B. (2011). *NCHRP 24-27(01): Evaluation of bridge pier scour research: scour processes and estimation*. Final report for NCHRP.

Ettema, R., Ng, K., Chakradhar, R., Fuller, J., & Kempema, E. W. (2015). Failure of spill-through bridge abutments during scour: Flume and field observations. *Journal of Hydraulic Engineering, 141(5),* 06015001.

Ettema, R., Constantinescu, G., & Melville, B. W. (2017). Flow-field complexity and design estimation of pier-scour depth: Sixty years since Laursen and Toch. *Journal of Hydraulics Engineering*, *143*(9), 03117006.

Hoffmans, G. J., & Verheij, H. J. (1997). *Scour manual* (Vol. 96). A.A. Balkema, Rotterdam, Netherlands.

Hong, S. H., and Abid, I. (2019). Scour around an erodible abutment with riprap apron over time. *Journal of Hydraulic Engineering, 145(6),* 06019007.

Horna-Munoz, D. and Constantinescu, G. (2018). A fully 3-D numerical model to predict flood wave propagation and assess efficiency of flood protection measures. *Advances in Water Resources, 122*, 148-165.

Horna-Munoz, D. and Constantinescu, G. (2020) 3-D dam break flow simulations in simplified and complex domains, *Advances in Water Resources*, *137*, 103510, https://doi.org/10.1016/j.advwatres.2020.103510.

Koken, M., & Constantinescu, G. (2014). Flow and turbulence structure around abutments with sloped sidewalls. *Journal of Hydraulic Engineering*, *140*(7). 04014031.

Kothyari, U.C., Hager, W.H. and Oliveto, G. (2007). Generalized approach for clearwater scour at bridge foundation elements, *Journal Hydraulic Engineering, 133(11),* 1229-1240.

Lagasse, P, Zevenberger,L., Schall, J and Chopper, P. (2001). *Bridge scour and stream instability countermeasures: experience, selection, and design guidance: Hydraulic Engineering Circular No. 23* (FHWA-NH1-01-003). National Highway Institute (US).

Melville, B. W. and Coleman, S. E. (2000). *Bridge scour.* Water Resources Publications, Littleton, Colorado.

Melville, B., van Ballegooy, S., Coleman, S. and Barkdoll, B. (2006a). Countermeasures to protection at spill-through abutments. *Journal of Hydraulic Engineering*, *132*:235-245.

Melville, B., van Ballegooy, S., Coleman, S. and Barkdoll, B. (2006b). Scour countermeasures for wing wall abutments. *Journal of Hydraulic Engineering, 132*:563-574.

Melville, B., Van Ballegooy, S., Coleman, S. and Barkdoll, B. (2007). Riprap selection at wing wall abutments. *Journal of Hydraulic Engineering,133*:1265-1269.

NCHRP Project 24-18 (*NCHRP Report 587*), *Countermeasures to Protect Bridge Abutments from Scour.*

NCHRP Project 24-19, *Selection Criteria and Design Guidelines, and techniques for the Size and Placement of Environmentally Sensitive Channel and Bank Protection Measures, and Quality Control.*

NCHRP Project 24-20, *Prediction of Scour at Bridge Abutments*.

Pagaz-Ortiz, J. (1991). *Stability of rock riprap for protection at the toe of abutments located at the flood plain, Rep. No. FHWA-Rd-91-057*, Federal Highway Administration, US Dept. of Transportation, Washington, DC.

Roulund, A., Sumer, M., Fredsoe, J. ad Michelsen, J. (2005). Numerical and experimental investigations of flow and scour around a circular pile. *Journal of Fluid Mechanics, 534,* 351-401.

Sturm, T. W., & Janjua, N. S. (1994). Clear water scour around abutments in floodplains. *Journal of Hydraulic Engineering*, *120*(8), 956-972.

Sturm, T. W., Ettema, R., & Melville, B. W. (2011). *Evaluation of bridge-scour research: Abutment and contraction scour processes and prediction (pp. 24-27).* Washington, DC, USA: National Cooperative Highway Research Program, Transportation Research Board of the National Academies.

Sumer, B. M. and Fredsoe J. (2002). *The mechanics of scour in the marine environment*. World Scientific.

Wu, H., Zeng, J. and Constantinescu, G. (2020). A multi-parameter design formula for riprap size selection at wing-wall abutments, *Journal Hydraulic Research*, paper TJHR-2019-0218, https://doi.org/10.1080/00221686.2020.1818310.

Wu, H., Zeng, J. and Constantinescu, G. (2021). A design formula for sizing rock riprap at spill-through abutments in compund channels, *Journal Hydraulic Engineering*, 147(10), https://doi.org/10.1061/(ASCE)HY.1943-7900.0001919.

Zeng, J., Constantinescu, G., Blanckaert, K., & Weber, L. (2008). Flow and bathymetry in sharp open-channel bends: Experiments and predictions. *Water Resources Research*, *44*(9), W09401.